Li Z, Xu K, Wang Z, Bi K, Qin H, Giaralis A (2024) Analytical design of non-grounded tuned mass damper inerter for base-excited structures, *International Journal of Mechanical Sciences*, accepted, 15/5/2024.

Analytical Design of Non-grounded Tuned Mass-Damper-Inerter for Base-excited Structures

Zhenchuan Li [a], Kun Xu [a*], Zixiao Wang [b*], Kaiming Bi [c], Huailei Qin [a], Agathoklis Giaralis [d,e]

[a] State Key Laboratory of Bridge Safety and Resilience, Beijing University of Technology, Beijing, 100124, China

[b] School of Electrical, Electronic, and Mechanical Engineering, University of Bristol, UK

[c] Department of Civil and Environmental Engineering, The Hong Kong Polytechnic University, Kowloon, Hong Kong, China

[d] Department of Civil Infrastructure & Environmental Engineering, Khalifa University, Abu Dhabi, UAE

[e] Department of Engineering, City, University of London, UK

*Correspondence: xukun@bjut.edu.cn (Kun Xu), zixiao.wang@bristol.ac.uk (Zixiao Wang)

Abstract: This paper contributes novel analytical formulae for H_∞ optimal tuning of non-grounded tuned mass-damper-inerter (TMDI) for minimizing free-end displacement of base-excited primary structures. The derivation relies on the fixed-point theory, making use of single-mode modelling of the primary structure while accommodating any arbitrary TMDI placement along the structure height. Optimal TMDI tuning parameters are derived for given dominant mode shape of primary structure and TMDI inertial properties (i.e., secondary mass and inertance) under two different types of harmonic excitations with frequency-independent displacement and acceleration amplitudes. The applicability of the derived TMDI tuning formulae for response mitigation of lightly damped primary structures under stationary broadband support excitation is established through comparisons with numerically optimal TMDI properties for a wide range of TMDI inertial properties. Moreover, the analytical TMDI tuning formulae derived in this study achieve enhanced structural performance for

base-excited structures compared to those from the literature, derived under various modelling assumptions and optimality criteria. Lastly, the potential of the proposed TMDI tuning for structural response mitigation is numerically evaluated by examining displacement, acceleration, and energy dissipation response history data of an experimentally identified reinforced concrete bridge pier model subjected to 100 earthquake ground motion (GM) records. Overall, reported results demonstrate that the derived analytical formulae can significantly extend the practical application of TMDI as a bona fide dynamic vibration absorber for base-excited structures by circumventing the need for computationally demanding numerical TMDI tuning optimization.

Keywords: Optimal structural vibration control, Base-excited cantilevered structures, Seismic response mitigation, Non-grounded tuned mass damper inerter, Analytical fixed-point optimal tuning, Seismic energy dissipation.

1 Introduction

In recent years, passive inerter-based dynamic vibration absorbers (IDVAs) have attracted significant research attention for the vibration control of dynamically excited structures [1-3]. The effectiveness of IDVAs relies on leveraging the inertial property of a two-terminal mechanical element, termed inerter [4], in order to amplify either the secondary oscillatory mass of tuned mass dampers (TMDs) [5] and/or the energy-dissipative capability of viscous dampers [6]. These benefits are enabled by the scalability of the inertial property, termed inertance, by which the inerter element resists the relative acceleration across its two terminals. Technologically, the inertance property can be materialized by various mechanics, including mechanical gearing [7-10], living hinges [11], electromagnetic principles [12], hydraulics pumps [13, 14], and fluid dynamic principles [15-17]. By virtue of any of these mechanics, inerter devices may be manufactured whose inertance can well be

orders of magnitude higher than their physical mass [18]. Typical configurations of IDVAs include the tuned viscous mass damper (TVMD) [6], rotational inertia double tuned mass damper (RIDTMD) [19], tuned inerter damper (TID) [20], tuned mass damper inerter (TMDI) [5], tuned liquid column damper inerter (TLCDI) [21], tuned tandem mass damper inerter (TTMDI) [22], lever-arm tuned mass damper inerter (LTMDI) [23-25], grounded inerter-based two-degree-of-freedom tuned mass damper (GI-TDOF-TMD) [26], tuned cable-inerter system (TCIS) [27], and tuned liquid inerter damper (TLID) [28, 29].

Among the above IDVA configurations, the tuned mass damper inerter (TMDI) has been extensively studied for mitigating dynamic responses in wind-excited tall buildings [30-33], long-span bridges [34-37], and wind turbines [38, 39], as well as in engineering structures subjected to base/seismic excitations, including buildings [40-43], wind turbines [44], and base-isolated structures [45-48]. The TMDI consists of a conventional TMD paired with an inerter device; the latter connects the secondary oscillatory mass either to the ground (grounded TMDI configuration) [49], or to the primary structure (non-grounded TMDI configuration). In non-grounded TMDIs, the inerter may be configured parallel to the viscoelastic connection of the secondary mass (parallel TMDI configuration) [50], in which case the secondary mass is linked to the primary structure at a single location, or the inerter may link the secondary mass to a different location of the primary structure from the location of the viscoelastic connection (non-parallel TMDI configuration) [51]. In the latter case, the TMDI is attached to primary structure at two distinct locations with different kinematics. Regardless of the TMDI configuration, the TMDI tuning principles are the same and fairly similar to the TMD tuning since the TMD can be interpreted as a TMDI with zero inertance [5]. In particular, TMD(I) tuning involves optimizing its viscoelastic properties (i.e., stiffness and damping) given inertial properties

(i.e., secondary mass and inertance) to achieve effective kinetic energy dissipation from the primary structure [5, 52]. Consequently, the control efficiency of TMDI heavily depends on the chosen tuning strategy.

In this regard, various numerical optimization approaches for TMDI tuning have been developed in recent years [53-56]. However, their implementation involves significant computational effort, which hinders their applicability in expeditious parametric investigations and structural performance assessments at preliminary structural design stages. The latter limitation is particularly important for non-grounded TMDI whose structural response mitigation capability depends heavily on the dominant mode shape of the primary structure, hence on the design of the primary structure [33, 55, 57]. To this end, analytical closed-form TMDI tuning expressions, relying on simplified structural and excitation models, are practically useful for facilitating TMDI implementation in various structural control applications.

In this respect, several studies contributed analytical tuning formulae for various TMDI configurations in different force-excited primary structures applications. Specifically, Hu and Chen [50] derived analytical formulae for tuning parallel TMDIs subjected to harmonic and white-noise excitations using H_∞ and H_2 optimization criteria, respectively. Zhang and Fitzgerald [38] addressed the edgewise vibration of wind turbine blades using parallel TMDI by deriving analytical tuning formulae assuming harmonic external forces applied to the blades. For non-parallel non-grounded TMDIs, Sarkar and Fitzgerald [39] derived analytical formulae for controlling vibrations of wind turbine towers under white-noise force excitation, while Su et al. [58] reported closed-form formulae for harmonic force excited slender cantilevered structures. Moreover, Zhang et al. [59] derived analytical tuning formulae for non-parallel non-grounded TMDIs which account for the effect of

background flexibility from higher non-resonant modes in multi-storey buildings, modelled as lumped-mass multi-degree-of-freedom (MDOF) systems. Further, Xu et al. [34] determined the equivalent damping ratio of TMDI-equipped bridges and derived a design formula for controlling vortex-induced vibrations of bridge decks, while Chen et al. [60] derived the equivalent modal damping of flexible structures equipped with grounded TMDI and proposed analytical TMDI tuning formulae based on this derivation.

Nevertheless, research effort focusing on the derivation of analytical TMDI tuning formulae for base-excited primary structures is much more limited than for force-excited primary structures with relevant studies treating mostly TMDI configurations with grounded inerter. For example, Marian and Giaralis derived in [5] and in [61] analytical grounded TMDI tuning formulae for undamped single-degree-of-freedom (SDOF) primary structures under harmonic and white-noise base excitations based on H_2 and H_∞ optimality criteria, respectively, while analytical tuning approaches for various grounded TMDI configurations are reported in [62, 63] for base-isolated primary structures under white-noise excitation. In this regard, there is a lack of simplified analytical tuning expressions for non-grounded TMDI configurations in base-excited non-isolated cantilevered structures. Notably, the consideration of non-grounded TMDI configurations is the most relevant for fixed-based cantilevered structures since, in this class of structures, the peak structural response is commonly attained at the free-end. This observation calls for connecting the TMDI secondary mass via the viscoelastic link as close to the tip of the primary structure as possible, similarly to conventional TMD implementations. In this setting, it is practically challenging for the inerter device to reach all the way to the ground, therefore non-grounded TMDI configurations are most applicable.

To this end, this paper aims to fill the above identified gap in the literature by contributing novel

closed-form analytically derived expressions for optimal tuning of non-grounded TMDI for dynamic response mitigation of base-excited cantilevered structures. This pursuit is facilitated by adopting the generic 2-DOF model of TMDI-equipped cantilevered structures in [57] which allows for accommodating any arbitrary inerter connectivity in non-grounded TMDI configurations. In the adopted model, the primary cantilevered structure is represented by a single dominant mode which is a reasonable assumption since the dynamic response of cantilevered structures is mostly contributed by their first (fundamental) mode [39, 51, 58], even under broadband excitations [64]. Subsequently, the fixed-point theory, originally developed by Den Hartog [65], is applied to the 2-DOF system to derive closed-form expressions for optimal TMDI parameters that minimize the structure's free-end displacement under H_∞ optimality for harmonic base displacement excitation and for harmonic base acceleration with frequency-independent amplitude. The achieved level of structural response mitigation of the proposed TMDI tuning formulae is compared with several analytical tuning expressions from the literature derived for grounded TMDI in base-excited structures as well as for non-grounded TMDI in force-excited structures for a wide range of TMDI inertial properties. These comparisons establish the importance and practical usefulness of the herein derived formulae vis-à-vis previously derived tuning formulae for the case of grounded TMDI in base-excited structures and of non-grounded TMDI in force-excited structures. Further, comprehensive parametric analyses are undertaken to assess the accuracy of the derived TMDI tuning expressions compared to numerical tuning for lightly damped structures under harmonic and white noise base excitations. Finally, the robustness of the derived H_∞-optimal tuning formulae to uncertainty in the base-excitation properties is numerically assessed by statistically evaluating various dynamic performance metrics of a reinforced concrete bridge pier model with experimentally identified properties, subjected to three

different suites of recorded earthquake ground motions (GMs) with different frequency content prepared for the FEMA P659 report [66].

The remainder of the paper is organized as follows. Section 2 establishes the governing equations for the TMDI-equipped structure under fixed-amplitude displacement and acceleration harmonic base excitations. Employing the fixed-point theory, Section 3 derives closed-form expressions for H_∞-optimal TMDI tuning parameters. Section 4 assesses the accuracy and robustness of the derived TMDI tuning formulae for lightly damped structures under broadband excitation. Section 5 compares the structural performance achieved using the proposed TMDI tuning expressions versus analytical tuning expressions from the literature. Lastly, Section 6 quantifies the potential of the derived TMDI tuning expressions for earthquake engineering applications, while Section 7 summarizes the main conclusions of this study.

2 Modelling of TMDI-equipped cantilevered structures

This section presents the adopted generic dynamic modelling of fixed-based cantilevered structures equipped with a TMDI and establishes its governing equations of motion for displacement and acceleration harmonic base excitations with frequency-independent amplitudes. The dynamic model is utilized in Section 3 to derive novel analytical formulae for the optimal tuning parameters of the non-grounded TMDI in base-excited structures.

2.1 System description and dynamic modelling

Consider the generic cantilevered (primary) structure with height H shown in Fig. 1(a), subjected to a horizontal base excitation with acceleration trace $\ddot{y}_g(t)$, where a dot over a symbol denotes differentiation with respect to time t. Let $y(x,t)$ be the lateral relative displacement of the structure with respect to the ground (deflection) at height x, with $0 \leqslant x \leqslant H$. Further, assume that $y(x,t)$ can

be faithfully approximated by a single mode shape such that $y(x,t) = \phi(x)y_s(t)$, where $\phi(x)$ is a deformation (shape) function which satisfies the fixed-end boundary conditions and $y_s(t)$ is the free-end structural deflection. In this regime, the primary structure can be modelled as a generalized SDOF system with mass, M_s, inherent damping coefficient, C_s, and stiffness, K_s, given as

$$M_s = \int_0^H m(x)\phi^2(x)\,dx\ , C_s = 2M\omega_s\xi_s\ , \text{and}\quad K_s = \int_0^H EI(x)\left(\frac{d^2\phi(x)}{dx^2}\right)^2 dx, \tag{1}$$

where $m(x)$ and $EI(x)$ are the distributed mass and the flexural rigidity along the height of the primary structure, respectively, while ω_s and ξ_s are the generalized system natural frequency and critical damping ratio, respectively.

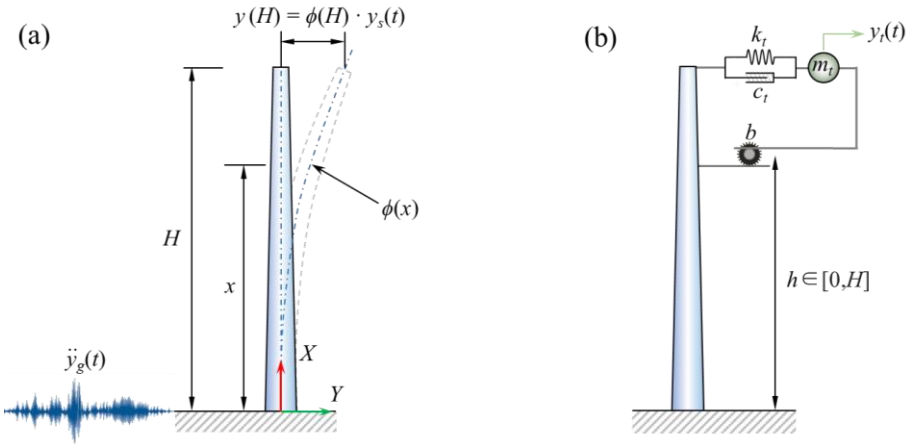

Fig. 1 Base-excited cantilevered structure (a) without TMDI and (b) equipped with TMDI.

In this work, a TMDI is considered to suppress the lateral motion of the considered primary structure. The TMDI comprises a secondary mass m_t attached to the free-end of the primary structure via a linear spring with stiffness coefficient k_t in parallel connection with a linear dashpot with damping coefficient c_t as shown in Fig. 1(b). Further, the secondary mass is also supported to the primary structure at height h $(0 \le h \le H)$ by an ideal inerter element with inertance coefficient b. By assuming that the primary structure is sufficiently stiff such that the shape function $\phi(x)$ is not

influenced by the presence of the TMDI, the lateral motion of the TMDI-equipped structure can be defined using the structural free-end deflection, y_s, and the TMDI stroke, y_d=$y_t - y_s$, that is, the secondary mass deflection relative to the primary structure free-end deflection. Therefore, the adopted modelling assumptions results in a 2-DOF dynamic system [57].

2.2 Equations of motion

The governing equations of the TMDI-equipped structure in Fig.(1b) modelled as detailed in the previous section are written as

$$M\ddot{y}_s + C\dot{y}_s + Ky_s = -M_e\ddot{y}_g + \phi(H)F_t + \phi(h)F_b \tag{2}$$

and

$$m_t(\ddot{y}_s + \ddot{y}_d) = -m_t\ddot{y}_g - F_t - F_b, \tag{3}$$

where $M_e = \int_0^H m(x)\phi(x)\,dx$ and F_b and F_t are the resisting forces of the inerter and of the damper exerted to the primary structure at heights h and H, respectively, given as

$$F_t = k_t y_d + c_t\dot{y}_d \text{ and } F_b = b\ddot{y}_d. \tag{4}$$

Consider the cases of harmonic base displacement and acceleration excitations with frequency ω defined as [67]

$$y_g = y_{g,0}\cdot e^{i\omega t} \text{ and } \ddot{y}_g = \ddot{y}_{g,0}\cdot e^{i\omega t}, \tag{5}$$

respectively, where $i = \sqrt{-1}$ and $u_{,0}$ is the amplitude of u quantity. Notably, in Eq.(5) the amplitude of the ground acceleration, $\ddot{y}_{g,0}$, is frequency-independent (i.e., $\ddot{y}_{g,0} \neq \omega^2 y_g$), which ensures the applicability of H_∞ optimal TMDI tuning, pursued in the next section, for acceleration ground motion with pre-specified amplitude across all the excitation frequencies. Under any of the two excitations in Eq.(5), the response of the 2-DOF system governed by Eqs.(2) and (3) is also harmonic with

$$y_s = y_{s,0} \cdot e^{i\omega t} \text{ and } y_d = y_{d,0} \cdot e^{i\omega t}. \tag{6}$$

Then, by introducing the following five dimensionless system parameters: TMDI frequency ratio, υ_t, TMDI critical damping ratio, ξ_t, mass ratio, μ, inertance ratio, β, and effective modal mass ratio, γ, defined by

$$\upsilon_t = \frac{\sqrt{\frac{k_t}{m_t+b}}}{\omega_s}, \xi_t = \frac{c_t}{2(m_t+b)\omega_t}, \mu = \frac{m_t}{M_s}, \beta = \frac{b}{M_s}, \text{and } \gamma = \frac{M_e}{M_s} = \frac{\int_0^H m(x)\phi(x)\,dx}{\int_0^H m(x)\phi^2(x)\,dx}, \tag{7}$$

the equations of motion in Eqs. (2) and (3) can be written in matrix form as

$$\begin{aligned} &-\Omega^2 \begin{bmatrix} 1+\mu+\left(1-\phi(h)\right)^2\beta & \mu+\left(1-\phi(h)\right)\beta \\ \mu+\left(1-\phi(h)\right)\beta & \mu+\beta \end{bmatrix} \begin{Bmatrix} y_{s,0} \\ y_{d,0} \end{Bmatrix} \\ &+i\Omega \begin{bmatrix} 2\xi_s & 0 \\ 0 & 2(\mu+\beta)\upsilon_t\xi_t \end{bmatrix} \begin{Bmatrix} y_{s,0} \\ y_{d,0} \end{Bmatrix} + \begin{bmatrix} 1 & 0 \\ 0 & (\mu+\beta)\upsilon_t^2 \end{bmatrix} \begin{Bmatrix} y_{s,0} \\ y_{d,0} \end{Bmatrix} = \begin{Bmatrix} \gamma+\mu \\ \mu \end{Bmatrix} L \end{aligned} \tag{8}$$

where $\Omega = \omega/\omega_s$, and $L = \Omega^2 y_{g,0}$ for harmonic base displacement excitation and $L = -\ddot{y}_{g,0}/\omega_s^2$ for harmonic base acceleration excitation with frequency-independent amplitude. Note that in deriving Eq. (8), the mode shape normalization $\phi(H)$=1 has been taken to simplify the analytical work, without loss of generality.

It is important to note that the herein adopted dynamic formulation of the TMDI-equipped primary structure allows for modelling the grounded TMDI configuration and the non-grounded parallel TMDI configuration as special cases by setting $\phi(h)$=0 and $\phi(h)$=1 in Eq.(8), respectively. As discussed in the introduction, the above two TMDI configurations have been heavily studied in the literature for base excited primary structures modelled as lumped-mass SDOF systems [5, 46, 50, 61]. The latter class of primary structures can be readily modeled by setting γ=1 in Eq.(8). Further, the case of a conventional TMD can be retrieved by setting β=0 in Eq. (8). In the following sections, Eq. (8) is used to determine analytically two different objective functions for optimal H_∞ tuning of TMDI

in the general case of $0 \leq h \leq H$ and $\gamma \neq 1$.

3 Proposed analytical H_∞-optimal TMDI tuning

In this section, closed-form expressions for H_∞-optimal TMDI tuning parameters are presented using the 2-DOF dynamic modelling of a generic cantilevered TMDI- equipped structure. Two different optimization problem formulations are introduced in Section 3.1, which adopt the same design variables (TMDI tuning parameters) but utilize different objective functions. Both the objective functions can be analytically evaluated as detailed in Appendix A. In Section 3.2, closed-form expressions for the H_∞-optimal TMDI tuning parameters are reported, derived using fixed-point theory as detailed in Appendix B. The generality of these expressions is demonstrated using analytical H_∞ optimal tuning formulae from the literature for specific TMD(I) configurations.

3.1 Formulation of the optimization problem

Given TMDI inertial property ratios μ and β in Eq.(7) and primary structure shape function value $\phi(h)$, the proposed optimal TMDI tuning involves determining the TMDI frequency ratio, υ_t, and critical damping ratio, ξ_t, in Eq. (7) to minimize the structural displacement amplitude under harmonic base excitation. Herein, analytical expressions for the optimal TMDI parameters under harmonic base excitations are pursued, assuming that the structural damping is negligible compared to the supplementary damping provided by the TMDI (i.e., ξ_s=0) [68]. To this aim, two different objective functions (OFs), considered by Tsai and Lin [67], are adopted, corresponding to the two different types of harmonic base excitation in Eq.(5). The first, OF_1, is defined as the magnitude of the complex ratio $y_{s,0}/y_{g,0}$ (i.e., structural displacement amplitude over amplitude of the harmonic displacement base excitation). The second, OF_2, is defined as the magnitude of the complex ratio $y_{s,0}/\ddot{y}_{g,0}$ (i.e., structural displacement amplitude over frequency-independent amplitude of the

harmonic acceleration base excitation) multiplied by ω_s^2. Mathematically, the optimal tuning problem for the displacement base excitation can be written as

$$\min_{\upsilon_t,\xi_t}\left\{\mathrm{OF}_1=\left|\frac{y_{s,0}}{y_{g,0}}\right|\right\},\ \text{given}\ \ \mu,\ \ \beta,\ \ \phi(h) \tag{9}$$

and the optimal tuning problem for the acceleration base excitation can be written as

$$\min_{\upsilon_t,\xi_t}\left\{\mathrm{OF}_2=\omega_s^2\left|\frac{y_{s,0}}{\ddot{y}_{g,0}}\right|\right\},\ \text{given}\ \ \mu,\ \ \beta,\ \ \phi(h). \tag{10}$$

In this junction, it is important to note that the numerator in Eq. (10) should not be interpreted as structural acceleration amplitude as the term ω_s^2 in the numerator is solely included to ensure that OF_2 is dimensionless [61, 67].

The OFs in Eqs. (9) and (10) can be readily evaluated by the analytic expressions provided in Appendix A for ξ_s=0. Using these expressions, OF_1 and OF_2 are plotted in Fig.2 in the form of frequency response functions (FRFs), that is, with respect to the excitation frequency ratio, Ω, for three TMDI damping ratios, ξ_t. Both sets of FRFs are seen to intersect at two fixed excitation frequency ratios, i.e., Ω_P and Ω_Q, which are independent of ξ_t. In light of this, the classical fixed-point theory [65, 68] can be used to derive closed-form expressions for the optimal TMDI frequency and damping ratios. The derivations are detailed in Appendix B.

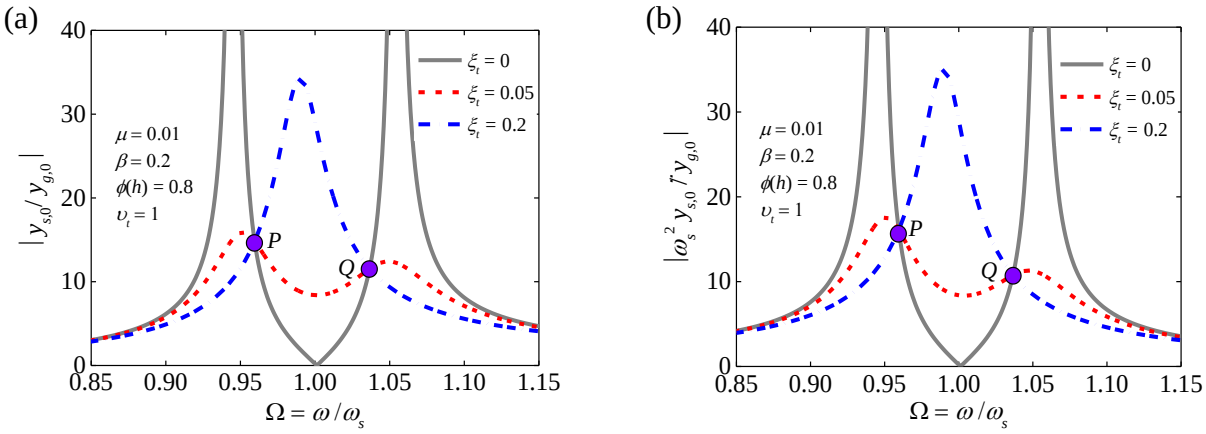

Fig. 2 Normalized structural displacement FRF curves for (a) OF_1 and (b) OF_2. The curves are plotted with the following parameters: mass ratio μ=0.01, inertance ratio β=0.2, TMDI frequency ratio υ_t=1, shape function $\phi(h)$=0.8, shape-specific effective modal mass ratio γ=1, and TMDI damping ratios ξ_t=0, 0.05 and 0.2.

3.2 Analytical expressions for H_∞-optimal TMDI tuning

Analytical expressions for the optimal TMDI tuning parameters and corresponding OF minimal values derived by application of the fixed-point theory to the optimization problems in Eqs.(9) and (10) are summarized in Table 1 (see Appendix B for the detailed derivations). The achieved optimality through the fixed-point theory approach is commonly regarded as H_∞ since it minimizes the OF values at the resonant frequency of the uncontrolled structures (Ω=1) [65]. To this end, for the sake of comparison, Table 2 reports optimal H_∞ tuning formulae previously derived in the literature for undamped lumped-mass SDOF structures under harmonic base excitation equipped with different TMD(I) configurations. It is found that all the tuning formulae of Table 2 are special cases of the herein derived optimal tuning expressions in Table 1. In particular, by setting β=0 (i.e., no inerter element) and γ=1 in Table 1, the analytical H_∞ optimal design formulae for the conventional TMD reported in [67] for OF_1 and in [52] for OF_2 are retrieved. Moreover, the H_∞ optimal design formulae for OF_2 and for grounded TMDI derived in [61] is obtained by setting $\phi(h)=0$ and γ=1 to the analytical expressions for OF_2 in Table 1.

Table 1 Closed-form formulae for H_∞ optimal TMDI tuning

OFs	$\upsilon_{t,opt}$	$\xi_{t,opt}$	Analytical expression of OFs
OF_1	$\sqrt{\dfrac{2a_3a_4-\mu a_1}{2a_2a_3a_4}}$	$a_1\sqrt{\dfrac{\mu^2a_2+a_4(5\mu a_1-6a_3a_4)}{8a_3a_4\left[\begin{matrix}\mu a_1a_2\\+a_4(a_1^2-2a_2a_3)\end{matrix}\right]}}$	$\left\lvert\dfrac{y_{s,0}}{y_{g,0}}\right\rvert=\dfrac{a_4\left(\begin{matrix}\sqrt{a_2}(2a_3a_4-\mu a_1)\\-a_1\sqrt{a_4(2a_3a_4-\mu a_1)}\end{matrix}\right)}{\sqrt{a_2}\left(\begin{matrix}a_1\sqrt{a_2a_4(2a_3a_4-\mu a_1)}\\-a_1^2a_4\end{matrix}\right)}$
OF_2	$\sqrt{\dfrac{2a_2a_3a_4}{\begin{matrix}-\mu a_1a_2-2a_1^2a_4\\2a_2^2a_3a_4\end{matrix}}}$	$a_1\sqrt{\dfrac{\begin{matrix}a_2a_4(6a_3a_4+\mu a_1)\\-(\mu a_2)^2-6(a_1a_4)^2\end{matrix}}{8a_2a_3a_4\left(\begin{matrix}2a_2a_3a_4\\-\mu a_1a_2-2a_1^2a_4\end{matrix}\right)}}$	$\left\lvert\dfrac{\omega_s^2y_{s,0}}{\ddot{y}_{g,0}}\right\rvert=\dfrac{1}{a_1}\sqrt{a_4\left(\begin{matrix}2a_2a_3a_4\\-\mu a_1a_2-a_1^2a_4\end{matrix}\right)}$

* a_1, a_2, a_3 and a_4 are given in Eq. (9)

Table 2 Previous analytical H_∞ optimal tuning formulae for specific TMD(I) configurations

OFs	Absorbers	$v_{t,opt}$	$\xi_{t,opt}$	Analytical expressions of OFs
OF_1	TMD (i.e., TMDI with β=0) [67]	$\frac{\sqrt{1+\mu/2}}{1+\mu}$	$\sqrt{\frac{3\mu}{8(1+\mu)}}$	$\left\|\frac{y_{s,0}}{y_{g,0}}\right\| = \sqrt{\frac{2+\mu}{\mu}}$
OF_2	TMD (i.e. TMDI with β=0) [52]	$\frac{\sqrt{1-\mu/2}}{1+\mu}$	$\sqrt{\frac{3\mu}{8(1+\mu)(1-\mu/2)}}$	$\left\|\frac{\omega_s^2 y_{s,0}}{\ddot{y}_{g,0}}\right\| = (1+\mu)\sqrt{\frac{2}{\mu}}$
OF_2	Grounded TMDI (i.e., TMDI with h=0) [61]	$\sqrt{\frac{(1+\mu)(2-\mu)-\mu\beta}{2(1+\mu+\beta)^2(1+\mu)}}$	$\sqrt{\frac{\beta^2\mu+6\mu(1+\mu)^2+\beta(1+\mu)(6+7\mu)}{8(1+\mu)(1+\mu+\beta)\cdot[2+\mu(1-\mu-\beta)]}}$	$\left\|\frac{\omega_s^2 y_{s,0}}{\ddot{y}_{g,0}}\right\| = \sqrt{\frac{(1+\mu)(\beta+2\mu+2)}{\mu+\beta}}$

To further demonstrate the generality of the analytical expressions in Table 1 to account for cantilevered structures with distributed mass/stiffness properties, Fig. 3 presents illustrative plots of the achieved minimum OF values and of the corresponding optimal TMDI parameters. These plots demonstrate that the well-known trends for lumped-mass primary structure (γ=1) reported in [61] hold for the case of distributed-mass continuous primary structures modelled as generalized SDOF systems (γ>1). Specifically, TMDI motion capability improves with inertance and/or mass ratios (β and μ), while the optimal TMDI frequency ratio reduces with μ and β, and the optimal TMDI damping ratio increases with μ and β. Further, Fig. 3 shows that the mass distribution of the cantilevered structure and the assumed dominant mode shape, as reflected on the γ value, has insignificant influence to the optimal TMDI frequency and damping properties, but affect significantly the TMDI control performance. In particular, for fixed TMDI inertial properties, higher γ, signifying skewed mass distribution towards the base of the primary structure, leads to higher OF values. These trends and observations echo the ones reported in [57], based on numerical optimization.

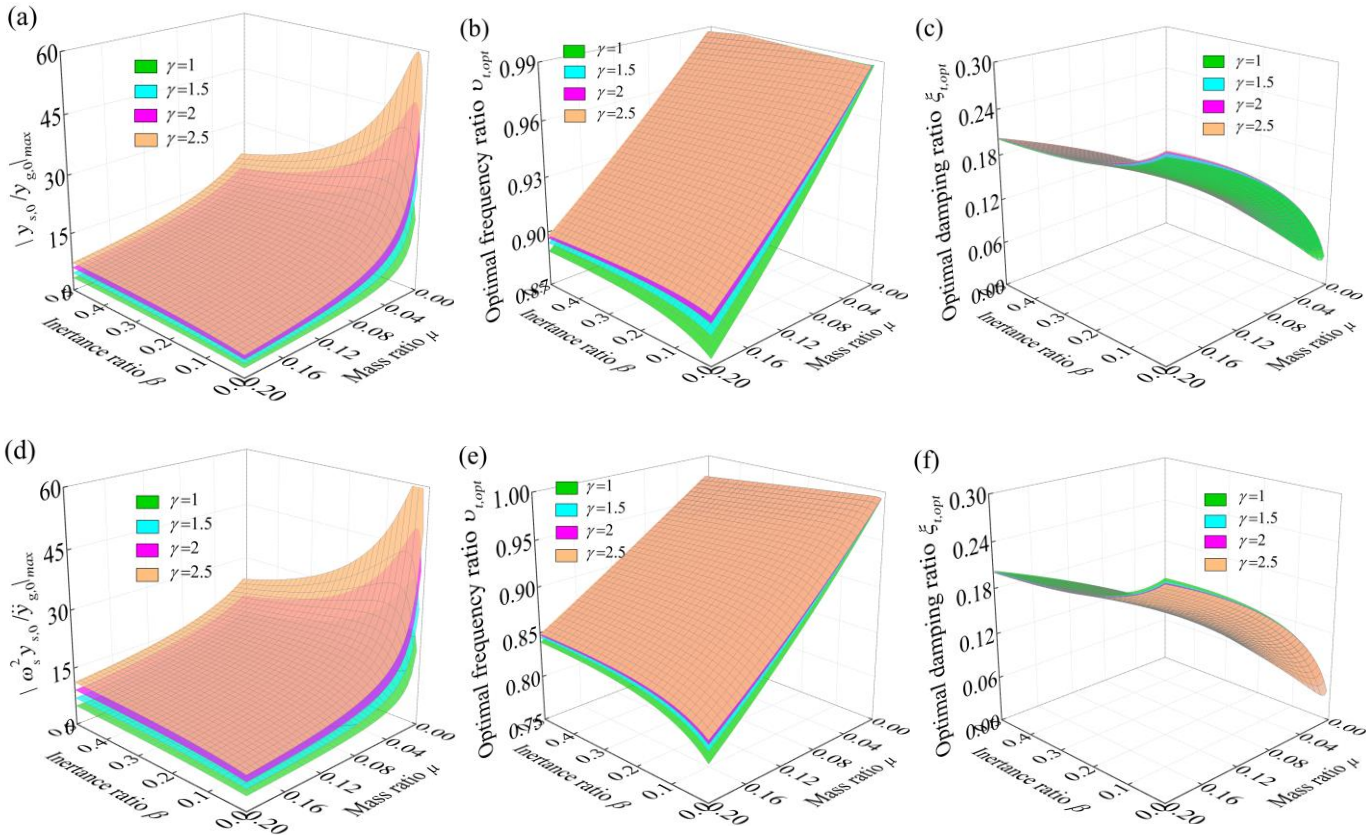

Fig. 3 Effects of the shape-specific effective modal mass ratio, γ, on normalized optimal FRF values and corresponding tuning parameters under conditions of fixed-amplitude displacement and acceleration base excitations. The upper panels (a-c) show the structural FRF values, optimal TMDI frequency ratios, and optimal TMDI damping ratios based on OF_1, each varying with mass and inertance ratios; the lower panels (d-f) show the corresponding values based on OF_2. The analyses consider mass ratio range μ=[0-0.2], inertance ratio range β=[0.005-0.5], effective modal mass ratio values γ=1, 1.5, 2 and 2.5, and a common shape function $\phi(h)$=0.8.

4. Applicability of proposed H_∞-optimal TMDI tuning for damped structures

The optimal TMDI tuning formulae in Table 1 assume no structural damping (ξ_s=0) and harmonic base excitations. This section evaluates the effectiveness of these formulae for vibration suppression in lightly damped structures, under both harmonic and white noise base excitations. To this aim, it compares the optimal tuning parameters and corresponding structural displacement FRF curves, derived analytically using expressions in Table 1, with those obtained through numerical solutions of optimal design problems, first for ξ_s=0 under harmonic excitations, and then for ξ_s≠0 under both

harmonic and white noise excitations.

4.1 Damped primary structures under harmonic excitation

First, the accuracy of the analytical formulae is assessed for the case of damped primary structures. To this end, two different optimal TMDI tuning problems are formulated aiming to minimize the maximum value of the two OFs considered in Section 3 for $\xi_s \neq 0$, which are mathematically written as

$$\min_{\upsilon_t,\xi_t}\left\{\max_{\Omega}\left[\mathrm{OF}_1 = \left|\frac{y_{s,o}}{y_{g,o}}\right|\right]\right\}, \text{ given } \mu,\ \beta,\ \phi(h) \tag{11}$$

and

$$\min_{\upsilon_t,\xi_t}\left\{\max_{\Omega}\left[\mathrm{OF}_2 = \omega_s^2\left|\frac{y_{s,o}}{\ddot{y}_{g,o}}\right|\right]\right\}, \text{ given } \mu,\ \beta,\ \phi(h) \tag{12}$$

The optimization problems in Eqs. (11) and (12) are numerically solved using the built-in Genetic Algorithm of MATLAB® with OF values analytically determined using the closed-form expressions in Appendix A.

In Fig. 4, the displacement FRF curves are plotted for OF_1 and OF_2 using the analytical expressions of Table 1 for undamped primary structure. Numerically obtained FRF curves derived from solving Eqs. (11) and (12) are superposed in Fig. 4. For both OFs, the FRF ordinates increase monotonically with β for the parallel TMDI configuration, that is, the parallel TMDI configuration is less effective than the conventional TMD which confirms previously reported data [50, 69]. However, FRF ordinates reduce with β for the non-parallel and grounded TMDIs confirming the improved vibration suppression capability of non-parallel TMDI configurations compared to TMD [53, 57]. More importantly, Fig. 4 demonstrates perfect matching between the FRF curves obtained through the numerical optimization and analytical formulae, confirming the accuracy of the derived expressions for undamped primary structure.

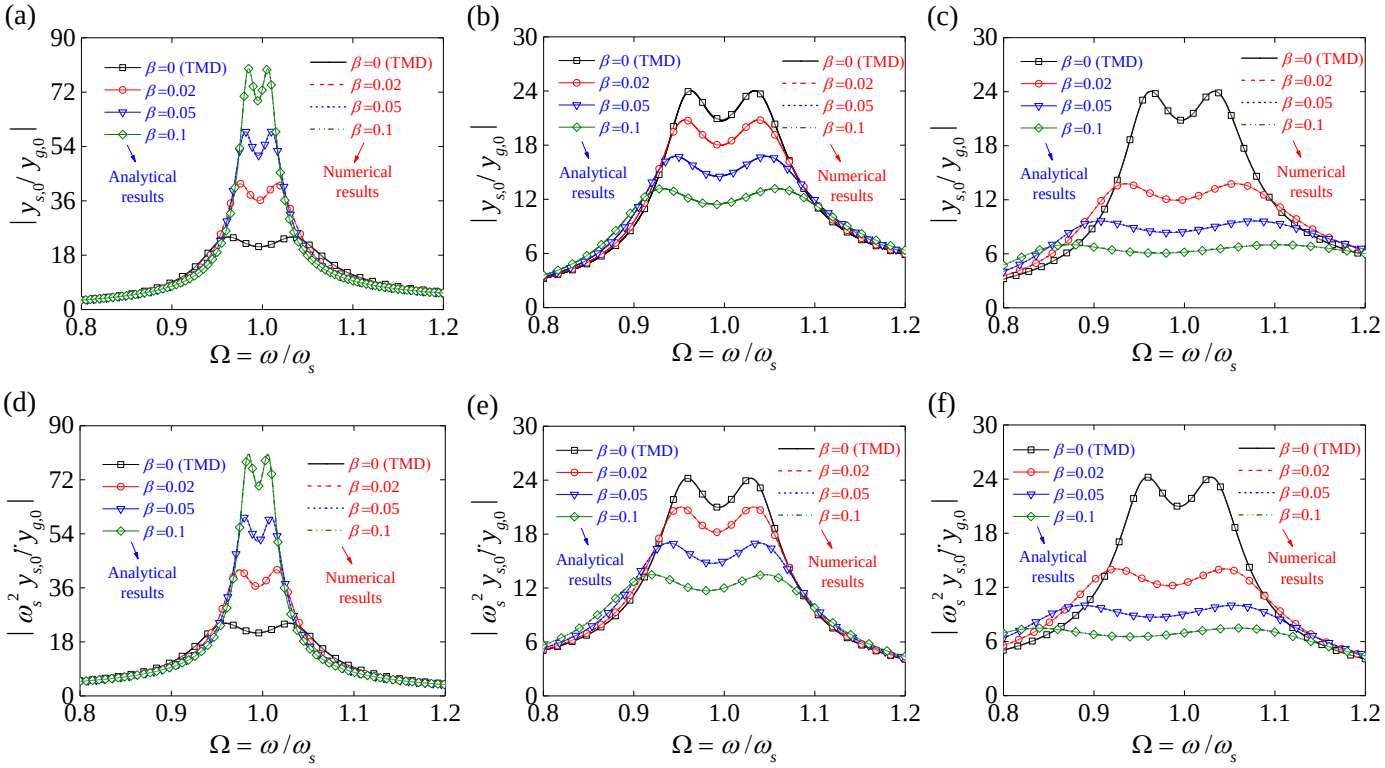

Fig. 4 Comparison of normalized structural displacement FRF curves derived from the analytical design formulae in Table 1 and those obtained through numerical optimization (with structural damping ratio ξ_s=0). The upper panels (a-c) show displacement FRF curves based on OF_1 under various inerter connectivity: (a) parallel TMDI with $\phi(h)$=1, (b) non-parallel TMDI with $\phi(h)$=0.5, and (c) grounded TMDI with $\phi(h)$=0. The lower panels (d-f) show the corresponding displacement FRF curves based on OF_2. The analyses employ a mass ratio μ=0.01, inertance ratio β=0, 0.02, 0.05 and 0.1, and an effective modal mass ratio γ=1.

Additionally, Fig. 5 plots the same type of results for the same TMDI properties but for damped primary structure with ξ_s=0.02. Expectedly, in this case, the analytical formulae of Table 1 are suboptimal as manifested by the fact that the two local maxima of all the analytically obtained FRFs in Fig. 5 do not attain the same maximum value, with the FRF value at the first resonant frequency being slightly higher than the FRF value of the second resonant frequency. Still, the analytical FRFs lie reasonably close to the FRF curves of the optimally designed TMDIs derived numerically by solving Eq. (10). These trends suggest that the proposed analytical formulae may be practically applicable for lightly damped structures (see also [70] for the case of conventional TMDs).

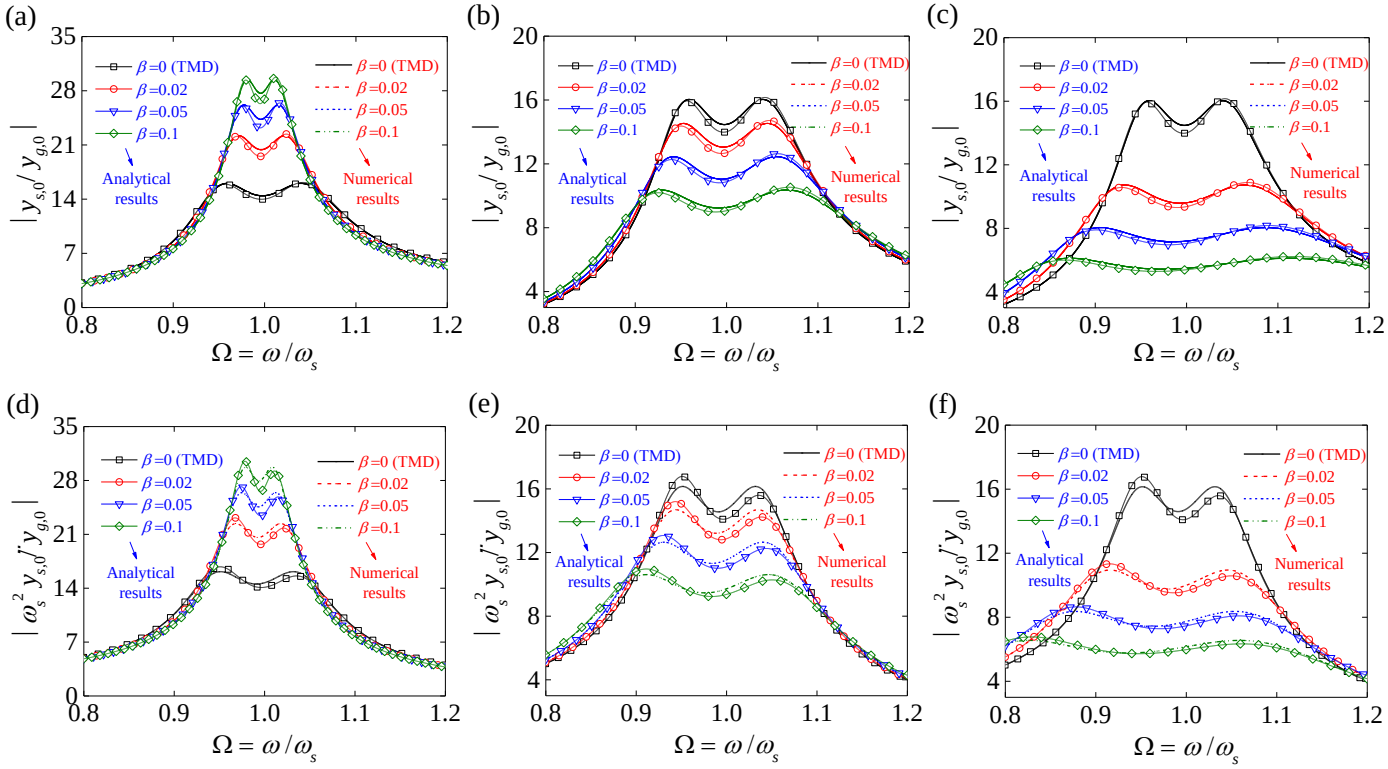

Fig. 5 Comparison of normalized structural displacement FRF derived from the analytical design formulae in Table 1 and those obtained through numerical optimization (with structural internal damping ratio ξ_s=0.02). The upper panels (a-c) show displacement FRF curves based on OF_1, employing the same inerter connectivity as used in Fig. 4. The lower panels (d-f) show the corresponding displacement FRF curves based on OF_2. The TMDI inertial properties are the same as those used in Fig. 4.

To demonstrate the potential applicability of the analytical formulae for lightly damped structures, further numerical results are provided in Figs. 6 and 7 plotting the discrepancy (error) between numerical TMDI frequency and damping properties for ξ_s=0.02, respectively, and analytically computed TMDI properties for undamped primary structure using the formulae in Table 1. That is,

$$Err_{\upsilon,t} = \frac{\upsilon_{t,analytical} - \upsilon_{t,numerical}}{\upsilon_{t,numerical}} \tag{13}$$

is plotted in Fig. 6 and

$$Err_{\xi,t} = \frac{\xi_{t,analytical} - \xi_{t,numerical}}{\xi_{t,numerical}} \tag{14}$$

is plotted in Fig.7.

Figure 6 shows that the error of the analytically optimal frequency ratios is practically negligible from the engineering viewpoint ranging within [-0.35%, +1.20%] for both OFs, with the formula for

OF_1 yielding consistently lower errors compared to the formula for OF_2. The larger error for OF_2 (i.e. +1.2% as opposed to -0.35% for OF_1) is manifested in Figs. 5(d-f) by a larger deviation of the equal local peak values in the FRFs for OF_2 obtained using the analytical tuning, compared to the negligible deviation for OF_1 in Figs. 5(a-c). Further, for OF_1, the percentage errors decrease as μ increases and/or as β decreases, while for OF_2, the percentage errors increase with increasing β for the practically important non-parallel TMDI configuration. Therefore, TMDI design using OF_2 frequency ratio formula with large inertance values should be used with caution.

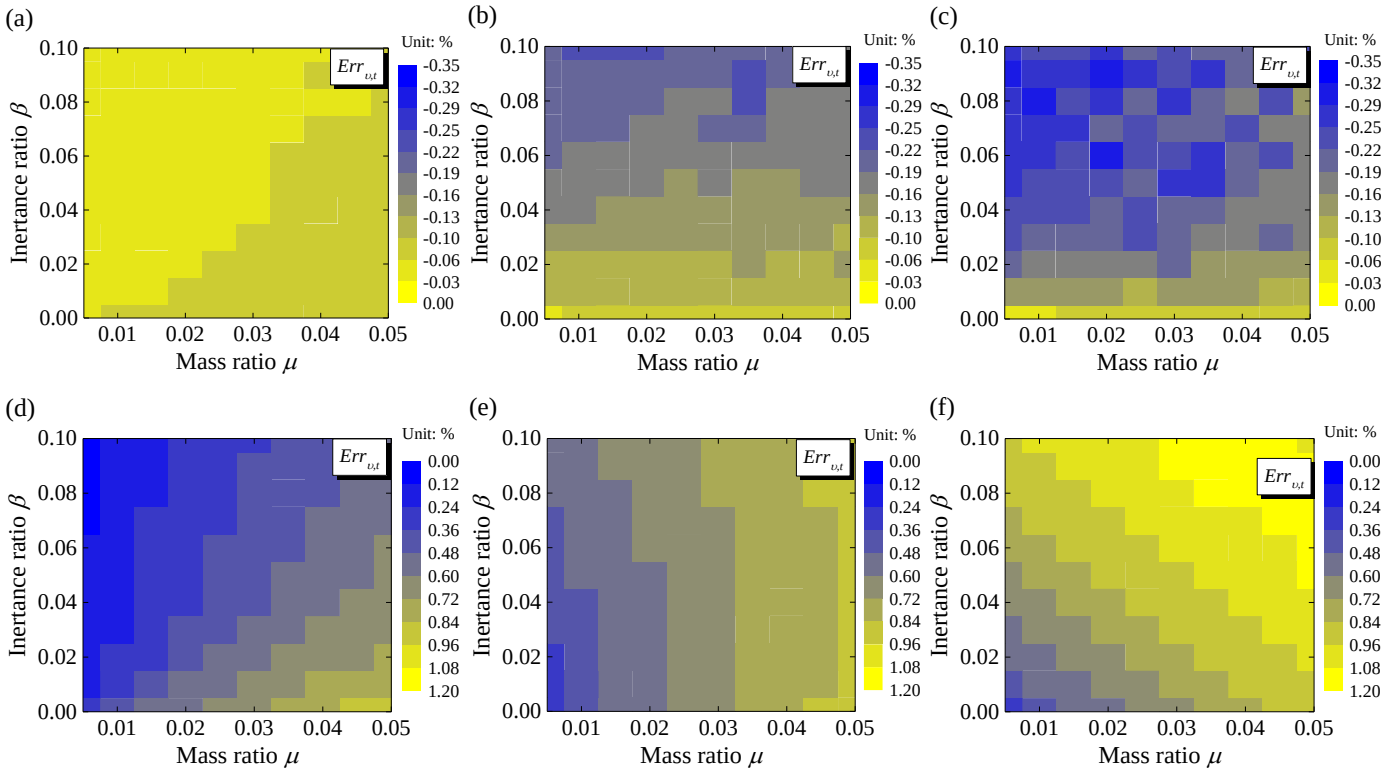

Fig. 6 Percentage errors between analytically and numerically derived optimal frequency ratios for two OFs, three TMDI configurations, and the damping ratio of ξ_s=0.02. The upper panels are the percentage errors of frequency ratios based on OF_1 at different inerter connectivity, (a) parallel TMDI $\phi(h)$=1, (b) non-parallel TMDI assuming $\phi(h)$=0.5, and (c) grounded TMDI $\phi(h)$=0, respectively. The corresponding percentage errors of frequency ratios based on OF_2 are depicted in (d-f) of the lower panels, respectively. The mass and inertance ratios are varied within the ranges [0.005, 0.05] and [0, 0.1], respectively.

Turning the attention to the errors in the TMDI damping ratio in Fig. 7, it is seen that unacceptably high errors (above 10%) are only attained for the practically least useful case of parallel TMDI

connection with very low secondary mass, $\mu \leq 1\%$. For the most beneficial TMDI configurations, the deviation of the TMDI damping ratio from the optimal value determined by the analytical formulae is consistently below 5% which is deemed acceptable.

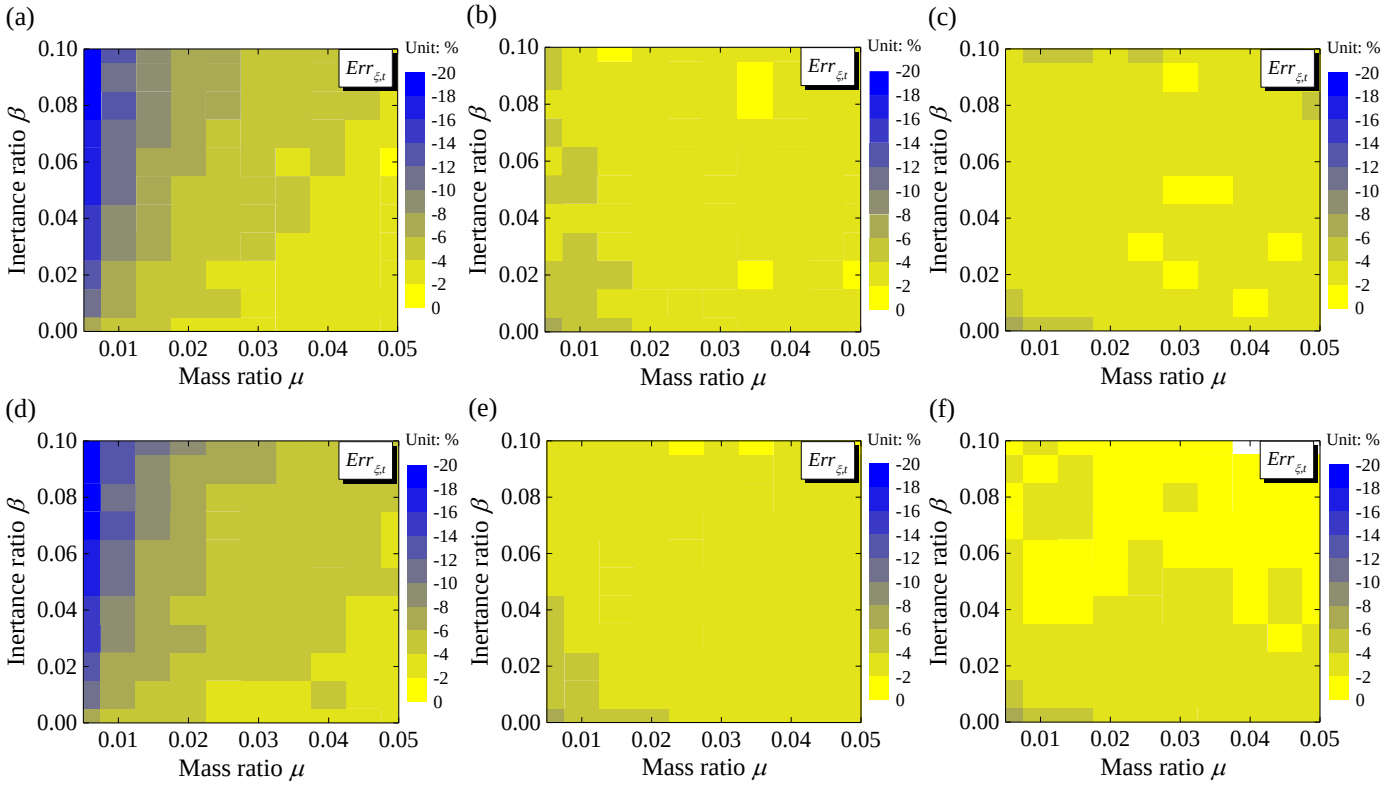

Fig. 7 Percentage errors between analytically and numerically determined optimal damping ratios for two OFs, three TMDI configurations, and the damping ratio of ξ_s=0.02. The upper panels are the percentage errors of damping ratios based on OF_1 at different inerter connectivity, (a) parallel TMDI $\phi(h)$=1, (b) non-parallel TMDI assuming $\phi(h)$=0.5, and (c) grounded TMDI $\phi(h)$=0, respectively. The corresponding percentage errors of damping ratios based on OF_2 are depicted in (d-f) of the lower panels, respectively. The TMDI inertial properties are same with those in Fig. 6.

4.2 Damped primary structures under white noise base excitation

Here, the applicability of the analytical TMDI formulae is assessed for damped structures, base-excited by stationary random white noise, taken as the extreme example of broadband excitation. To this aim, the TMDI performance is measured by the standard deviation of the free-end displacement of TMDI-equipped structure, normalized by the standard deviation of the free-end displacement of the uncontrolled structure. The adopted performance index is mathematically given as

$$J = \frac{\sigma_s}{\sigma_{un}} \tag{15}$$

where

$$\sigma_s = \sqrt{\int_{-\infty}^{+\infty} |H_s(\omega)|^2 S_0 d\omega} \quad \text{and} \quad \sigma_{un} = \sqrt{\int_{-\infty}^{+\infty} |H_{un}(\omega)|^2 S_0 d\omega} \tag{16}$$

in which $|H_s(\omega)|^2$ and $|H_{un}(\omega)|^2$ are the squared modulus of the free-end displacement transfer functions for the TMDI-controlled and uncontrolled structures and S_0 is the constant amplitude power spectral density function of the assumed ideal white noise.

Fig. 8 plots the performance index in Eq. (15) on the frequency ratio-damping ratio plane. The performance is significantly more sensitive with respect to the TMD(I) frequency ratio than with respect to the TMD(I) damping ratio. With increasing the structural damping ratio, the contribution of TMD(I) damping effect decreases, thus causing a reduction to the performance index in Eq.(15). Similar trend is reported for white noise force-excited TMDI-equipped structures [58]. Further, the performance of TMDI-equipped structure is superior to that of TMD-equipped structure. It is seen that the deviation of the OF_1 and OF_2 values of TMD(I) tuning parameters from the optimal values and the corresponding J index value is in the range of only 1% across all inherent critical damping ratios ξ_s considered. This fact showcases numerically that the proposed analytical TMD(I) tuning expressions can effectively support the TMD(I) design for vibration mitigation of damped primary structure under broadband (white-noise) base excitation.

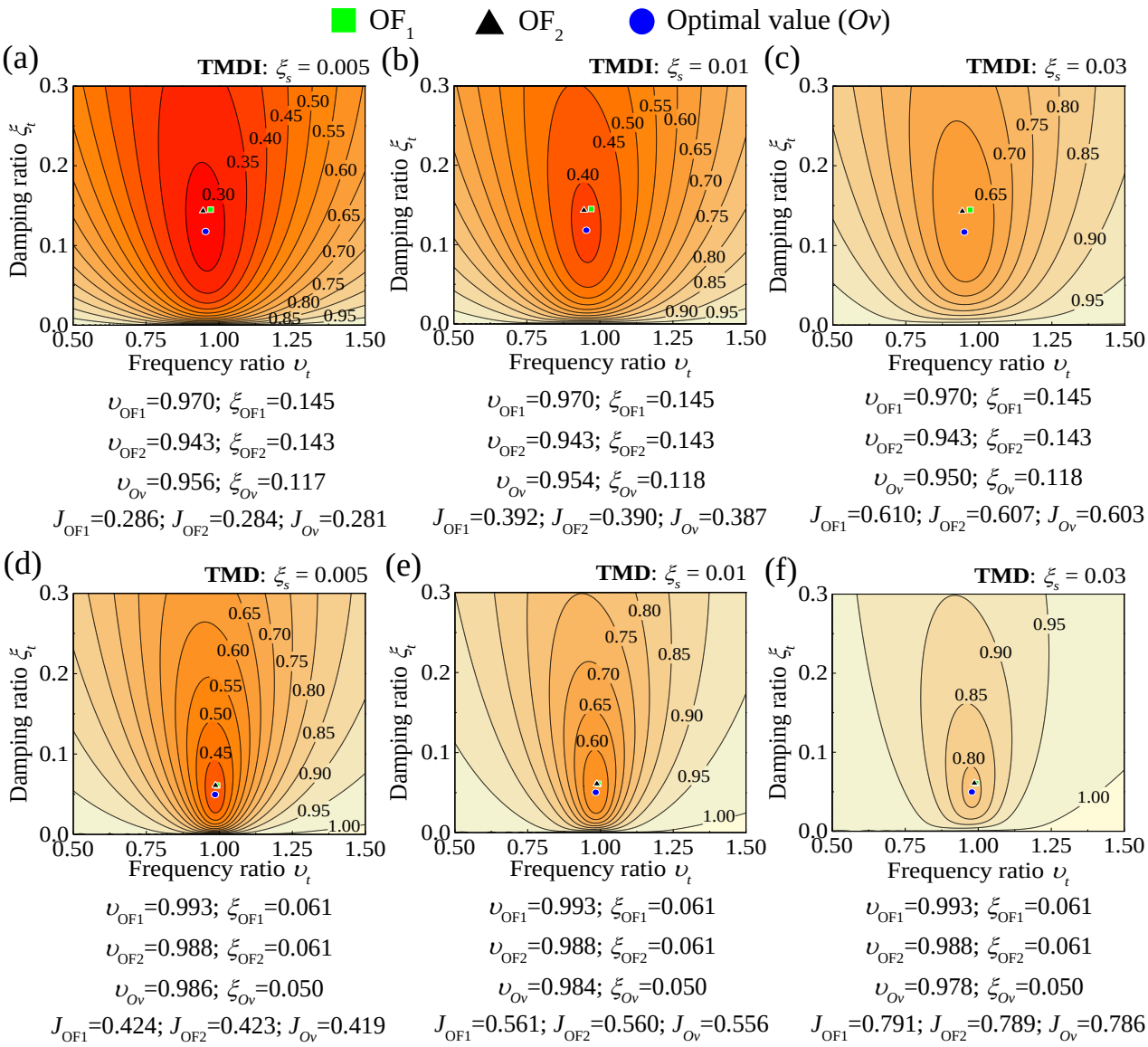

Fig. 8 Contour plots of control ratio with different structural damping ratios for TMD(I). (a-c) display the influence of TMDI frequency and damping ratios on the performance index in Eq. (13a) for structural damping ratios, ξ_s=0.5%, 1%, 3%, respectively; (d-f) examines the same for TMD design parameters with identical structural damping ratios. The mass ratio μ=0.01, inertance ratio β=0.2, and $\phi(h)$=0.5 for TMDI and the mass ratio μ=0.01 for TMD are adopted. The range of TMD(I) frequency and damping ratios are υ_t=[0.5, 1.5] and ξ_t=[0, 0.3], respectively. The shape-specific effective modal mass ratio γ=1. The locations of TMD(I) frequency and damping ratios obtained by the expressions based on OF_1 and OF_2, as well as the optimal locations of design parameters are marked by the square green, the triangular black, and the blue circle symbols, respectively. The corresponding performance index (J), and design parameters (υ and ξ) with subscripts 'OF_1', 'OF_2', and 'Ov' are reported under the panels.

5. Performance comparison of proposed tuning formulae for various TMDI configurations

In this section, the structural displacement performance under base excitation achieved by the TMDI tuning formulae in Table 1 is compared to that achieved by previous tuning formulae from the literature for the following three different TMDI configurations: 1) grounded TMDI $\phi(h=0)=0$ optimized based on H_2 and H_∞ criteria for lumped-mass SDOF structures under base excitation [5, 61], 2) parallel TMDI $\phi(h=H)=1$ optimized based on H_2 and H_∞ criteria for lumped-mass structures under force excitation [50], and 3) non-parallel TMDI $0<\phi(0<h<H)<1$ optimized based on empirical fitting and H_∞ optimal data for structures under force excitation [58, 71]. The purpose of these comparisons is to demonstrate and quantify the improved TMDI control performance accomplished by the herein proposed TMDI tuning formulae.

5.1 Grounded TMDI configuration $\boldsymbol{\phi(h=0)=0}$

Optimal tuning formulae for grounded TMDI in base-excited lumped-mass structures have been derived by Marian and Giaralis based on H_∞ [61] optimality (fixed-point theory approach) as

$$\upsilon_{t,opt}=\sqrt{\frac{(1+\mu)(2-\mu)-\mu\beta}{2(1+\mu+\beta)^2(1+\mu)}} \text{ and } \xi_{t,opt}=\sqrt{\frac{\beta^2\mu+6\mu(1+\mu)^2+\beta(1+\mu)(6+7\mu)}{8(1+\mu)(1+\mu+\beta)[2+\mu(1-\mu-\beta)]}}, \tag{14}$$

as well as based on H_2 [5] optimality (structural displacement variance minimization under white noise excitation) as

$$\upsilon_{t,opt}=\sqrt{\frac{[\beta(\mu-1)+(2-\mu)(1+\mu)]}{(1+\mu+\beta)\sqrt{2(1+\mu)}}} \text{ and}$$
$$\xi_{t,opt}=\frac{\sqrt{\mu+\beta}\sqrt{\beta(3-\mu)+(4-\mu)(1+\mu)}}{2\sqrt{2(1+\mu+\beta)[\beta(1-\mu)+(2-\mu)(1+\mu)]}} \tag{15}$$

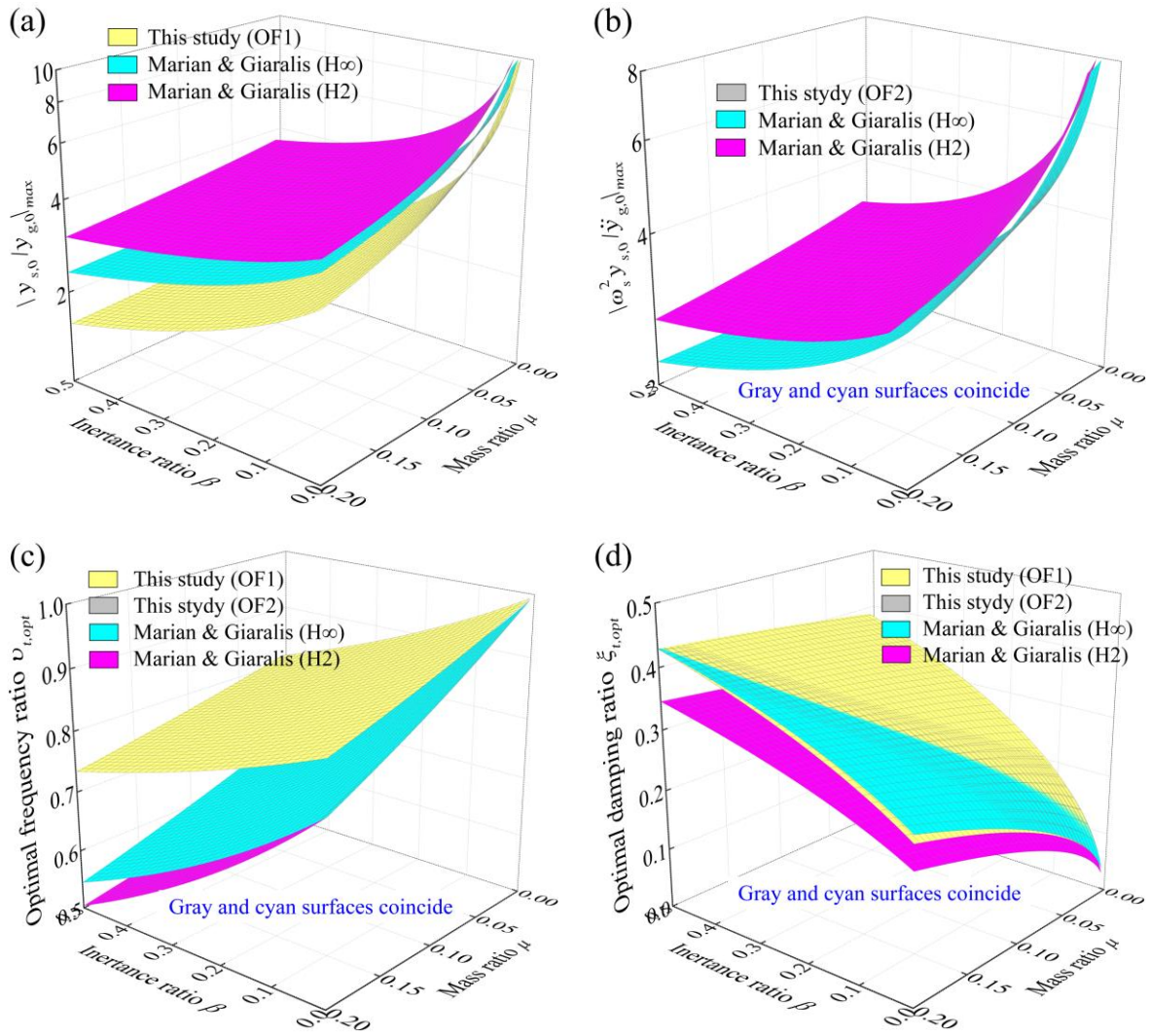

Fig. 9 Comparison of structural displacement FRF values and optimal parameters using different design formulae of grounded TMDI. (a) Displacement FRF value based on OF_1; (b) Displacement FRF value based on OF_2; (c) Frequency ratio of TMDI; (d) Damping ratio of TMDI. The TMDI design parameters are calculated using the formulae in Table 1, and in Eqs. (14) and (15) for mass ratio range μ=[0-0.2], inertance ratio range β=[0-0.5], and shape-specific effective modal mass ratio γ=1.

A comparison of the normalized displacement FRF values achieved by the above tuning formulae and the formulae in Table 1 is provided in Fig. 9. It is found that TMDI tuning using the herein derived expressions achieve significantly better performance in terms of OF_1 in Fig. 9(a) for all μ and β values (i.e., the yellow performance surface lies always lower than the other surfaces). This improvement stems from a higher frequency ratio obtained from the herein expressions as demonstrated in Fig. 9(c), as well as differences in the optimal damping ratios in Fig. 9(d). The OF_2 performance in Fig. 9(b) achieved by the expressions from this study is the same with the one achieved by the expressions derived by Marian and Giaralis [61] since the two sets of expressions are

same as noted in section 3.2 (i.e., the gray and cyan surfaces in Figs. 9(b-d) coincide). However, improved OF_2 performance from the expressions of this study is achieved compared to the performance of H_2 expressions in [5].

5.2 Parallel TMDI configuration $\boldsymbol{\phi(h=H)=1}$

For parallel TMDI configuration in force-excited lumped-mass structures, Hu and Chen [50] derived optimal tuning formulae based on H_∞ optimality (fixed-point theory approach) as

$$\upsilon_{t,opt} = \sqrt{\frac{\mu + (1+\mu)\beta}{(1+\mu)^2(\mu+\beta)}} \text{ and } \xi_{t,opt} = \sqrt{\frac{3\mu^2}{8(1+\mu)(\mu+\beta)}}, \tag{16}$$

as well as based on H_2 optimality (structural displacement variance minimization under white noise excitation) as

$$\upsilon_{t,opt} = \sqrt{\frac{[2\beta(1+\mu)+\mu(\mu+2)]}{2(1+\mu)^2(\mu+\beta)}} \text{ and}$$
$$\xi_{t,opt} = \sqrt{\frac{(\mu+\beta)+\upsilon_{t,opt}^4(\mu+\beta)(1+\mu)^2-\upsilon_{t,opt}^2\mu(\mu+2)-2\beta\upsilon_{t,opt}^2(1+\mu)}{4\upsilon_{t,opt}^2(\mu+\beta)(1+\mu)}}. \tag{17}$$

In Fig. 10, the performance in terms of OF_1 and OF_2 achieved by the above expressions is compared with the performance achieved by the TMDI tuning formulae in Table 1. It is seen in Figs. 10(a) and 10(b) that the OF_1 and OF_2 performances achieved by the tuning formulae derived in this study are consistently better than those achieved by Eqs.(16) and (17) for the full range of TMDI properties. Nevertheless, the improvement in performance offered by the herein derived formulae reduces as the mass ratio decreases. This trend can be attributed to the fact that as the TMDI mass ratio reduces, the difference in the dynamic response of force-excited and base-excited TMDI-equipped structures becomes less important.

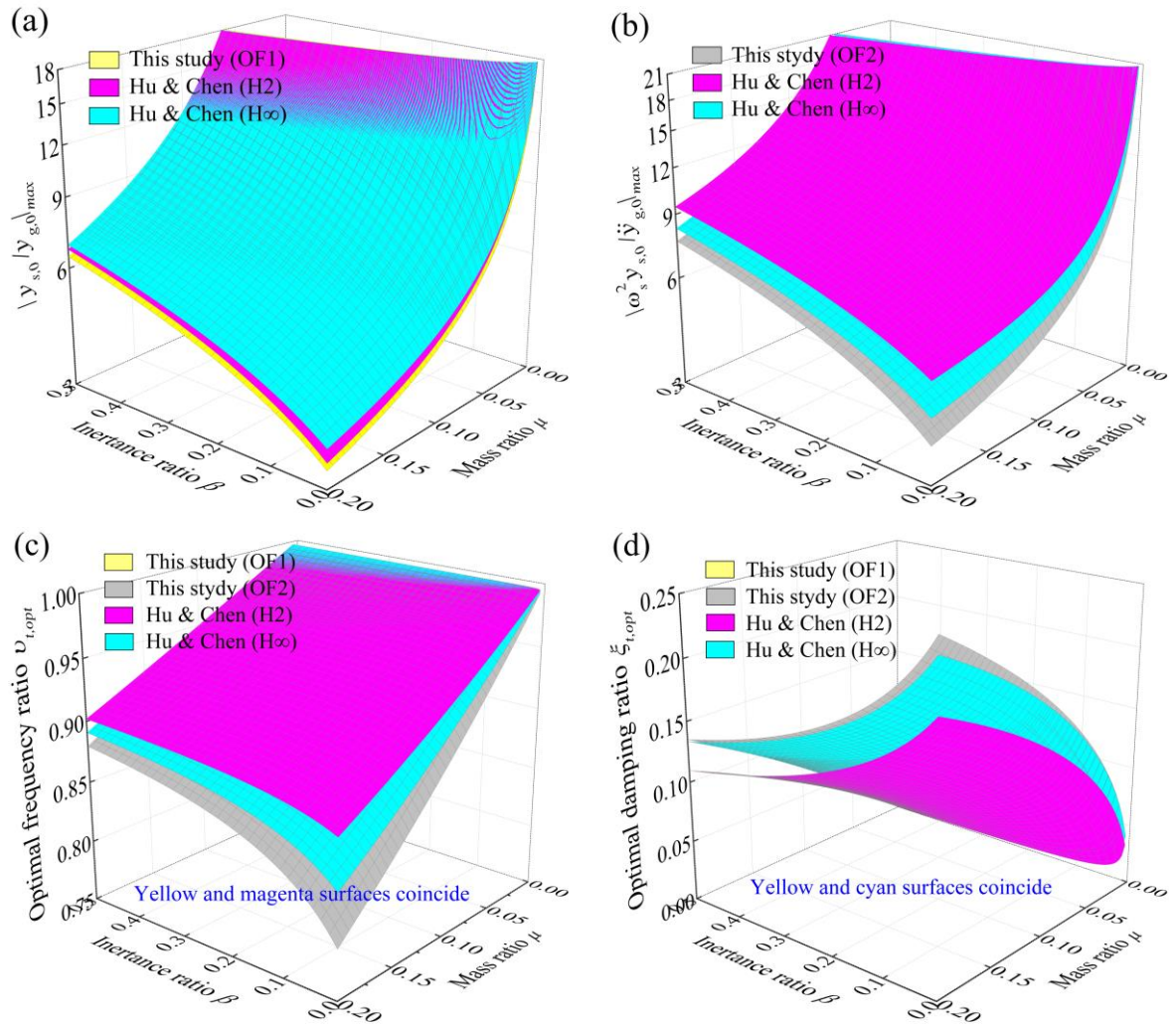

Fig. 10 Comparison of structural displacement FRF values and optimal parameters using different design formulae of parallel TMDI. (a) Displacement FRF value based on OF_1; (b) Displacement FRF value based on OF_2; (c) Frequency ratio of TMDI; (d) Damping ratio of TMDI. The TMDI design parameters are calculated using the formulae in Table 1, and in Eqs. (16) and (17) for mass ratio range μ=[0-0.2], inertance ratio range β=[0-0.5], and shape-specific effective modal mass ratio γ=1.

Still, the optimal frequency ratio expression for OF_1 criterion in this study coincides with that in Eq. (17) from Hu and Chen [50] for H_2 optimal tuning (i.e., the yellow and magenta surfaces in Fig. 10(c) coincide). Similarly, the optimal damping ratio expression for OF_2 criterion in this study coincides, with that in Eq. (16) from Hu and Chen [50] for H_∞ optimal tuning (i.e., the yellow and cyan surfaces in Fig. 10(d) coincide). In this regard, the tuning formulae of Hu and Chen [50] are special cases of the herein proposed ones in Table 1. However, the surfaces in Figs. 10(a) and 10(b) suggest that the use of the tuning formulae derived in this study should be used for base-excited

structures since in practice the mass ratio is non-negligible, even in cases of no intended secondary mass, as the actual TMDI device components, will always have some non-zero self-weight (e.g. [9, 47]).

5.3 Non-parallel TMDI configuration $0<\phi(0<h<H)<1$

For the most general case of non-parallel TMDI configuration, Su et al. reported TMDI tuning formulae accounting for the location of the inerter connection at height h, for force-excited cantilevered structures, using H_∞ optimality [58] (fixed-point theory approach) as

$$\upsilon_{t,opt}=\frac{\sqrt{1+\mu\beta\phi^2(h)/(\mu+\beta)}}{1+\mu+\beta\left(1-\phi(h)\right)^2} \text{ and } \xi_{t,opt}=\sqrt{\frac{3}{8}\frac{\mu+\beta\left(1-\phi(h)\right)^2-\mu\beta\phi^2(h)/(\mu+\beta)}{1+\mu+\beta\left(1-\phi(h)\right)^2}}, \tag{18}$$

as well as by empirical fitting [71] to numerically derived data as

$$\begin{aligned}\upsilon_{t,opt}&=\sqrt{\frac{1}{1+\mu+\beta\left(1-\phi(h)\right)^2}\cdot\frac{1}{1+(\mu+\beta)\left(1-\phi(h)\right)^2}}\ and\\ \xi_{t,opt}&=\frac{1}{4}\left(\sqrt{\frac{\mu+\beta(1-\phi(h))^2}{1+\mu+\beta(1-\phi(h))^2}}+\sqrt{\frac{(\mu+\beta)(1-\phi(h))^2}{1+(\mu+\beta)(1-\phi(h))^2}}\right).\end{aligned} \tag{19}$$

Pertinent results are provided in Fig. 11 to compare the achieved OF_1 and OF_2 performances and the underlying TMDI tuning parameters obtained from Eqs. (18) and (19) vis-à-vis the expressions in Table 1 derived in this study. As in all previous comparisons with tuning formulae from the literature examined, the TMDI tuning formulae proposed in this study achieve improved OF_1 and OF_2 performances than those achieved by Eqs. (18) and (19). Nevertheless, the improvement reduces for lower mass ratio values for the same reason explained in the previous sub-section. Looking at the optimal TMDI properties in Figs. 11(c) and 11(d), the values obtained by the expressions in this study are significantly different from the empirically fitted data by Su et al. [71], and also deviate from the H_∞ based expressions of Su et al. [58], except for very small values of mass ratio. In this respect, the

use of the formulae in Table 1 is recommended over Eqs. (18) and (19) for base-excited TMDI-equipped structures with non-negligible secondary mass ratios.

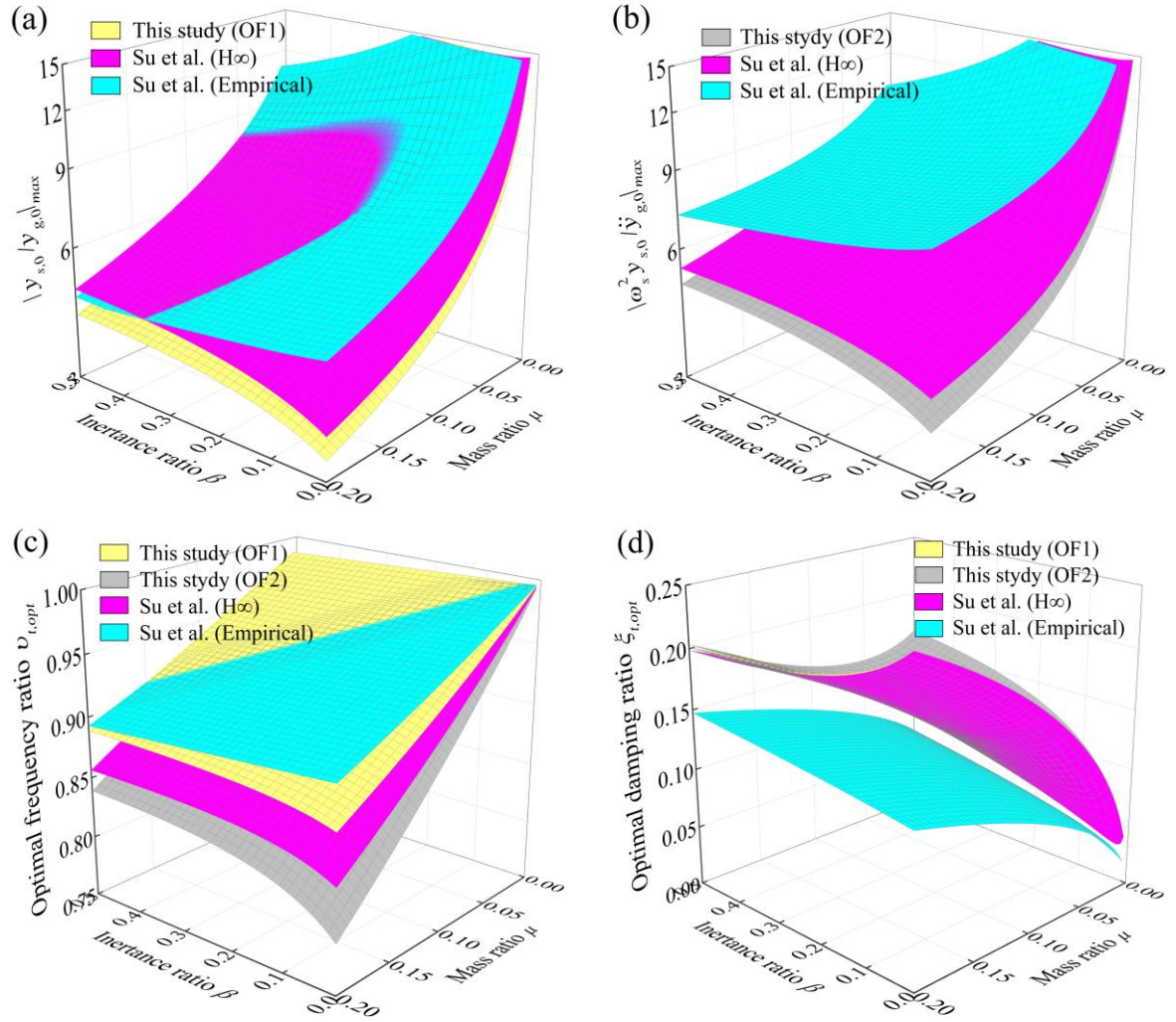

Fig. 11 Comparison of structural displacement FRF values and optimal parameters using different design formulae of non-parallel TMDI. (a) Displacement FRF value based on OF_1; (b) Displacement FRF value based on OF_2; (c) TMDI frequency ratio; (d) TMDI damping ratio. The TMDI design parameters are calculated using the formulae in Table 1, and in Eqs. (18) and (19) for mass ratio range μ=[0-0.2], inertance ratio range β=[0-0.5], shape-specific effective modal mass ratio γ=1, and shape function value $\phi(h)$=0.8.

As a closure to this section, Figs. 9-11 are collectively discussed vis-à-vis to draw some practically important observations on the optimal TMD(I) tuning parameters obtained in this study compared against to those obtained from formulae published in the literature. Specifically, it is seen that in some cases the herein proposed formulae require higher TMDI frequency and/or damping ratios. This is particularly evident for the grounded TMDI in Fig. 9(c), where noticeably higher optimal frequency

ratio values are obtained by using the tuning formulae for OF_1. Nevertheless, it should be noted that the herein obtained frequency ratio values are similar to those derived in the optimal design of conventional TMDs [67]. Further, this increase in the optimal frequency ratio is not observed in Figs. 10(c) and 11(c) for the parallel and non-parallel TMDI configurations, which are arguably more practical than the grounded TMDI. Meanwhile, the optimal TMDI damping ratios based on OF_2 for non-grounded TMDI configurations are only slightly larger than those calculated using previous formulae from the literature as shown in Figs. 10(d) and 11(d). For the remaining cases, the optimal TMDI parameters based on both OFs do not consistently yield the highest values among all compared design formulae. Interestingly, the optimal frequency ratios based on OF_2 for non-grounded TMDIs are the smallest as shown in Figs. 10(c) and 11(c). Collectively, the above observed trends in the optimal parameters yielded by the proposed formulae suggest that improved TMDI vibration suppression performance achieved is not associated with out-of-ordinary values for the TMDI stiffness and damping parameters. Therefore, the proposed TMDI tuning formulae in Table 1 are not expected to have adverse consequences to the manufacturability and/or upfront costs of the TMDI.

6 Performance assessment of proposed formulae under earthquake excitations

Having established the usefulness of the proposed tuning formulae in Table 1, this final section aims to demonstrate their applicability for transient non-stationary base excitations focusing on earthquake-induced ground motions (GMs). This is pursued by taking a large-scale model of a bridge pier from the literature as the benchmark structure, excited by a suite of 100 recorded GMs. For these GMs, statistical time domain response performance metrics and data from cumulative seismic energy dissipation analyses are presented for the primary structure equipped with TMDI tuned by both OF_1

and OF_2.

6.1 Benchmark primary structure and recorded ground motions

The scaled-down model of a double-column reinforced concrete bridge pier shown in Fig. 12(a) is adopted from [72] for numerically evaluating the seismic response mitigation performance of the TMDI tuned by the formulae in Table 1. This is supported by idealizing the bridge pier specimen as a SDOF system by lumping its total mass, M=6520 kg, at the girder location as shown in Fig. 12(b). The natural frequency and damping ratio of the bridge pier were identified in the linear elastic stage using the improved empirical wavelet transform in [72] to be ω_s=22.62 rad·s^{-1} and to vary within ξ_s= [0.03, 0.04], respectively. For conservatism, an inherent damping ratio of ξ_s=0.03 is herein employed. The TMDI inertial properties are chosen to be m_t=130.4 kg, corresponding to mass ratio μ=0.02, and b=652 kg, corresponding to inertance ratio β=0.1, with $\phi(h)$=0 which is a practically reasonable configuration for bridge applications [73]. Optimal TMDI parameters obtained by the formulae of Table 1 for OF_1 and OF_2 are reported in Table 3, for γ=1 which is consistent with the model in Fig.12(b).

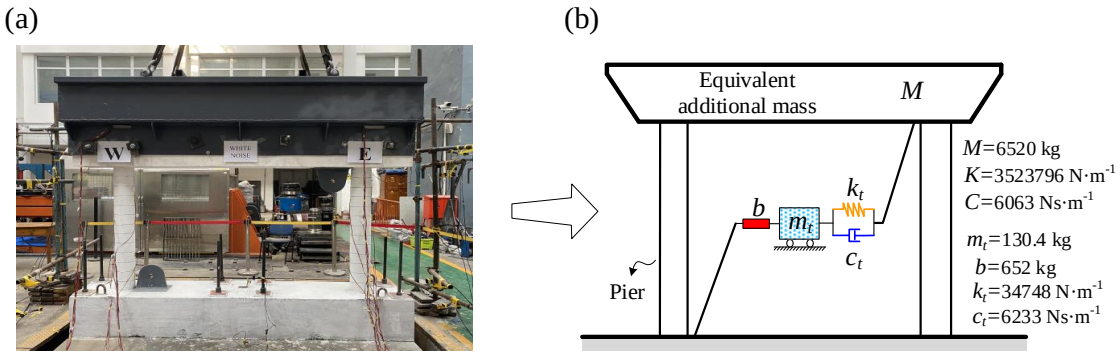

Fig. 12 (a) RC double-column bridge pier [72] and (b) its schematic equipped with TMDI.

Table 3 Design parameters of TMDI

	μ	β	$\phi(h)$	$\upsilon_{t,opt}$	$\xi_{t,opt}$
OF_1	0.02	0.1	0	0.9403	0.2054
OF_2				0.8879	0.2019

The seismic performance of the TMDI-equipped model of the benchmark structure in Fig. 12 is evaluated using 50 pairs of horizontal acceleration GM records with perpendicular directions per pair, i.e., 100 horizontal GMs in total, chosen from the Pacific Earthquake Engineering Research Center (PEER) database for FEMA P659 [66]. The GMs are classified in three different groups based on seismological criteria as follows: 28 near-fault GMs in 14 pairs without directivity pulse (NPNF), 28 near-fault GMs in 14 pairs with low-frequency pulse (PNF), and 44 far-field GMs in 22 pairs (FF). For the purposes of this study, all the GMs with peak ground acceleration (PGA) above $0.3g$, where g=9.81 m·s^{-2} is the gravitational acceleration, are uniformly scaled down to have PGA= $0.3g$. This scaling ensures that the linear structural behavior assumption holds for the adopted benchmark structure, based on shaking table testing in [72] showing no plastic deformation for excitations with PGA≤ $0.3g$. Acceleration response spectra of the unscaled GMs are shown in Fig. 13 alongside the median response spectrum of the unscaled and the scaled-down records, for each GM group.

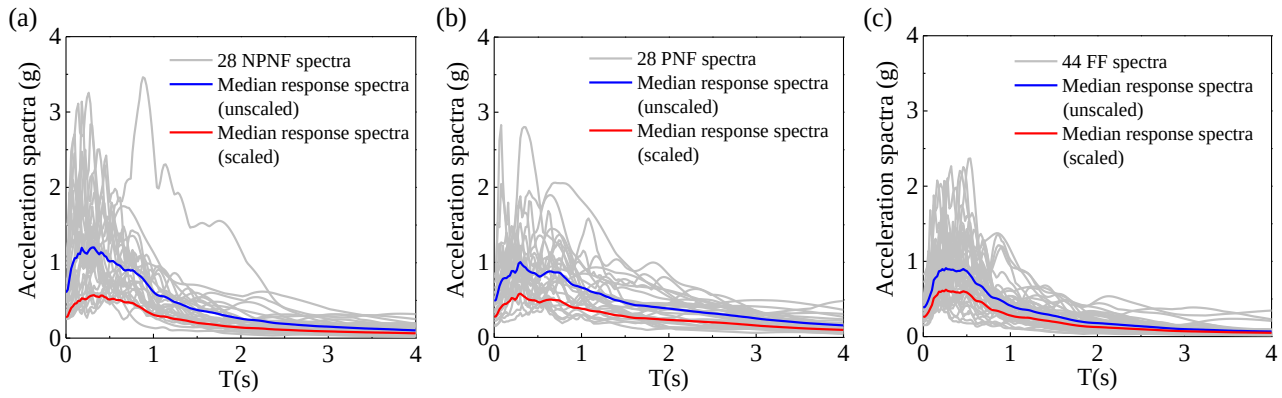

Fig. 13 Acceleration response spectra of 100 recorded GMs in FEMA P659 [66]. (a) 28 NPNF spectra; (b) 28 PNF spectra; (c) 44 FF spectra. Blue and red lines indicate the unscaled and scaled median response spectra, respectively. The scaled median response ensures that the linear elastic seismic response behavior assumption holds for the adopted benchmark structure.

Linear response history analysis is conducted to obtain numerically, by application of the Runge-Kutta method to Eqs. (2) and (3) written in state-space form, the response of the benchmark structure equipped with TMDI tuned by the formulae of Table 1 for the 100 scaled 100 GMs. In the remainder of this Section the performance of the considered system is assessed and discussed based on the thus obtained data.

6.2 Time-domain performance

The effectiveness of TMDI tuned by the expressions in Table 1 for seismic response mitigation of the benchmark structural model is herein evaluated by examining peak absolute structural displacement and acceleration data normalized by their corresponding values attained by the uncontrolled structure. The data are plotted in Fig. 14 for three GM groups in the form of percentage reduction ratios (i.e. higher values signify higher performance gains compared to the uncontrolled structure). Significant average response reductions in both structural displacement and acceleration for all GM groups are evidenced, despite the large record-to-record variability which is typical of recorded GMs (see also Fig. 13). Specifically, average response reduction of more than 26% is noted in terms of peak displacements and more than 30% in terms of peak accelerations for all GMs. Higher average response reductions are noted for the FF GM group, reaching more than 28% and 33% for peak displacements and accelerations, respectively. Moreover, average percentage reductions for near-fault GM groups are only slightly lower compared to the FF GM group which demonstrate that the TMDI tuned to the herein proposed formulae are robust to near-fault GM features, including low-frequency pulses. Indeed, there is insignificant difference of the average peak displacement reductions between the NPNF and PNF groups while average peak acceleration reductions of the PNF is very similar to that of the FF group. Further, there is very small difference in the achieved peak

response reductions across the groups for the two different TMDI tunings. Still, OF_2-based TMDI tuning achieves consistently higher average displacement reduction ratios than OF_1 while OF_1-based TMDI tuning achieves consistently higher average acceleration reduction ratios than OF_2 as shown by the reported COVs. In this regard, it is recommended to use the OF_2 formulae for TMDI tuning in Table 1 when structural displacement response mitigation is prioritized over acceleration response mitigation, which is commonly the case when structural damage risk reduction is deemed more essential from secondary equipment/traffic seismic risk reduction (see discussion in [74] and therein references).

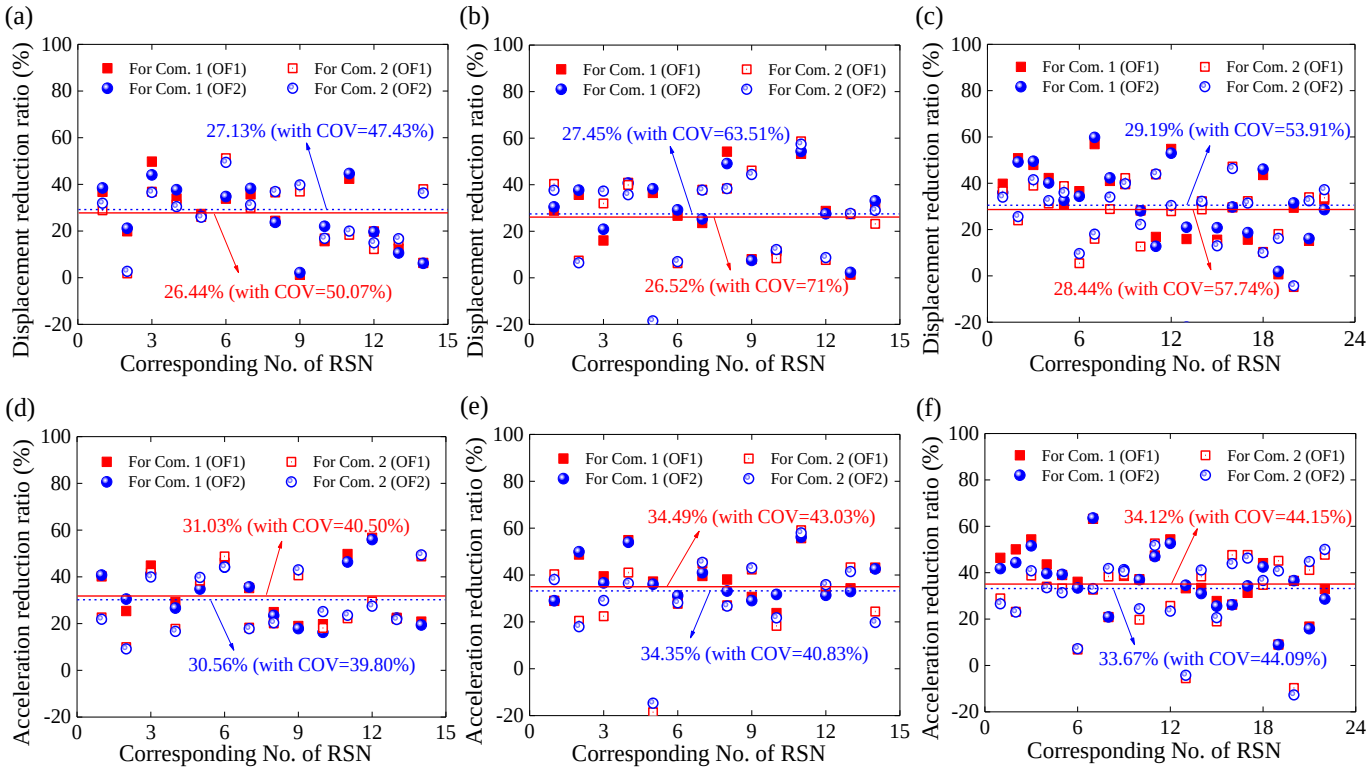

Fig. 14 Reduction ratios of peak structural displacement and acceleration achieved by TMDI. The upper panels (a-c) display the displacement reduction ratios under NPNF, PNF, and FF, respectively; the lower panels (d-f) show the corresponding acceleration reduction ratios. "RSN" refers to the GM record sequence number, while "Com. 1" and "Com. 2" denote the two perpendicular components of GM records. Horizontal solid and dashed lines represent the mean reduction ratios achieved by the TMDI tuned to OF_1 and OF_2 criteria, respectively.

To gain a further appreciation of the response reduction of TMDI tuned to the formulae of Table 1, Fig. 15 plots time histories of response structural displacement and acceleration for both TMDI-

controlled and uncontrolled structure under three different GMs, each one arbitrarily chosen from one of the three GM groups considered. The presented data show that the TMDI tuned to any of the two OF_1 and OF_2 criteria can effectively mitigate all the local maximum responses. Therefore, the tuned TMDI not only reduces the absolute peak responses (i.e., for the Kocaeli/Turkey event peak displacement response reduction are 58.6% for OF_1 and 57.4% for OF_2 while peak acceleration response reduction is 58.85% for OF_1 and 57.91% for OF_2) but also the temporal response averages (e.g. root mean square responses) which become important in reducing the risk of cumulative seismic damage. The latter issue is further examined in the following sub-section by looking into the seismic energy dissipation in time for the controlled and the uncontrolled structure.

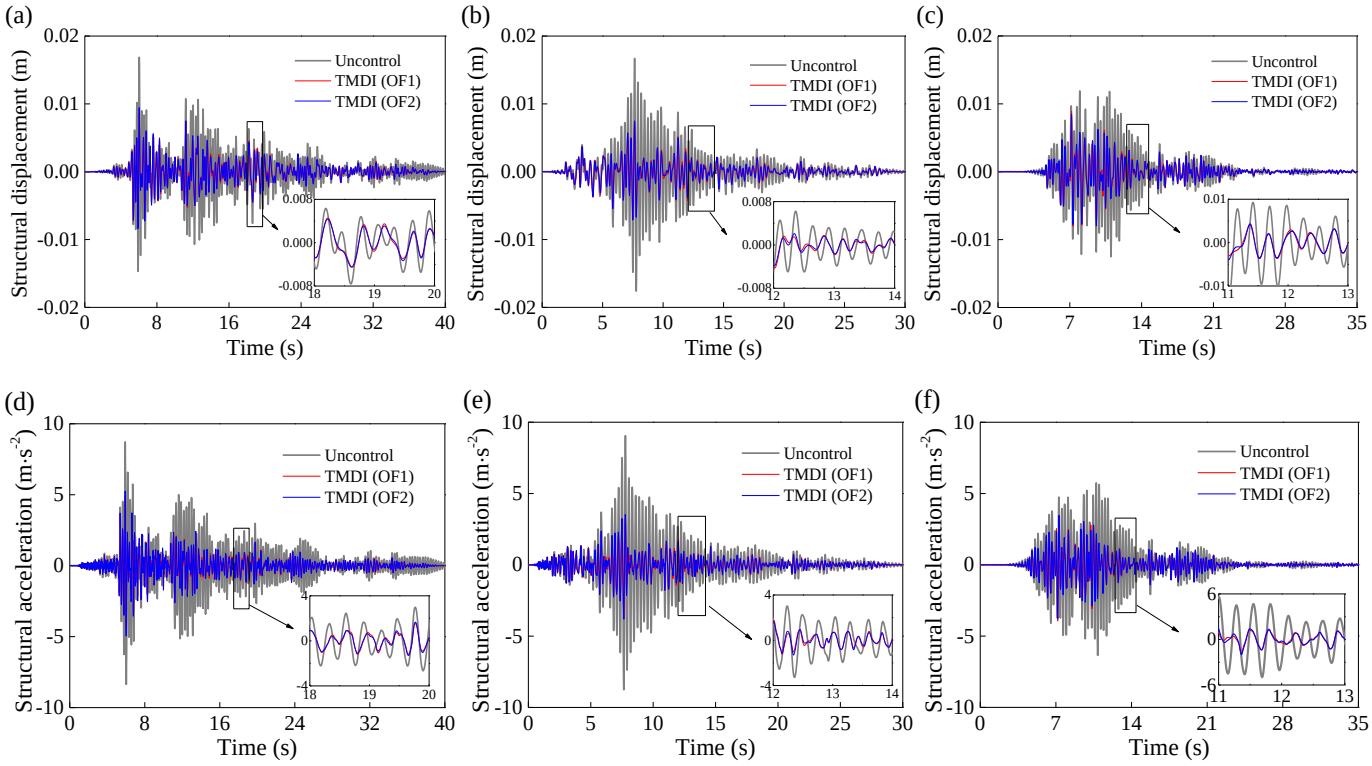

Fig. 15 Time histories of uncontrolled and TMDI-controlled structural displacement and acceleration under three GMs. The upper panels (a-c) show displacements under NPNF record #165 (Imperial Valley-06, PGA=0.28*g*), PNF record #1165 (Kocaeli, Turkey, PGA=0.22*g*), and FF record #1111 (Kobe, Japan, scaled PGA=0.3*g*); the lower panels (d-f) display the corresponding accelerations.

6.3 Seismic energy dissipation performance

Here, the cumulative temporal seismic energy dissipation capability of the TMDI tuned to the newly derived formulae of Table 1 is assessed. For this purpose, standard seismic energy balance considerations are employed [75]. Specifically, for the uncontrolled structure, the total input seismic energy, E_{C_un}, is equal to the dissipated energy through the inherent structural damping, that is,

$$E_{C\_un} = \int_0^t 2M\omega_s\xi_s[\dot{y}_s(t)]^2\,dt. \tag{20}$$

Further, for the TMDI-controlled structure, the total input energy, E_{C_con}, is dissipated through both the structural inherent damping, E_{C_s}, and the TMDI supplementary damping, E_{C_T}, [76], i.e.,

$$E_{C\_con} = E_{C\_s} + E_{C\_T} = \int_0^t 2M\omega_s\xi_s[\dot{y}_s(t)]^2\,dt + \int_0^t 2(m_t+b)\omega_t\xi_t[\dot{y}_d(t)]^2\,dt \tag{21}$$

The TMDI seismic energy dissipation performance is evaluated by examining the time histories of accumulated energy dissipated by the structure and by the TMDI as shown in Fig. 16. In the latter figure, time histories of accumulated seismic input energy and dissipated energy are normalized by the corresponding maximum accumulated energy, for the same GM records considered in Fig.15. As seen, the total input energy to the bridge pier is significantly reduced when a TMDI is deployed, irrespective of the tuning formulae used, though OF_1-based tuning appears to yield a slightly better performance. For instance, for TMDI tuned to OF_1 criteria the reductions in the total seismic input energy are 16.2%, 47.6%, and 18.4% with respect to the uncontrolled structure for the three GMs in Figs. 15(a-c), respectively. Further, most of the input seismic energy is dissipated by the TMDI. Indeed, approximately 78%, 87.5%, and 80% of the total seismic input energy are absorbed by the TMDI for the three GMs in Figs. 15(a-c), respectively.

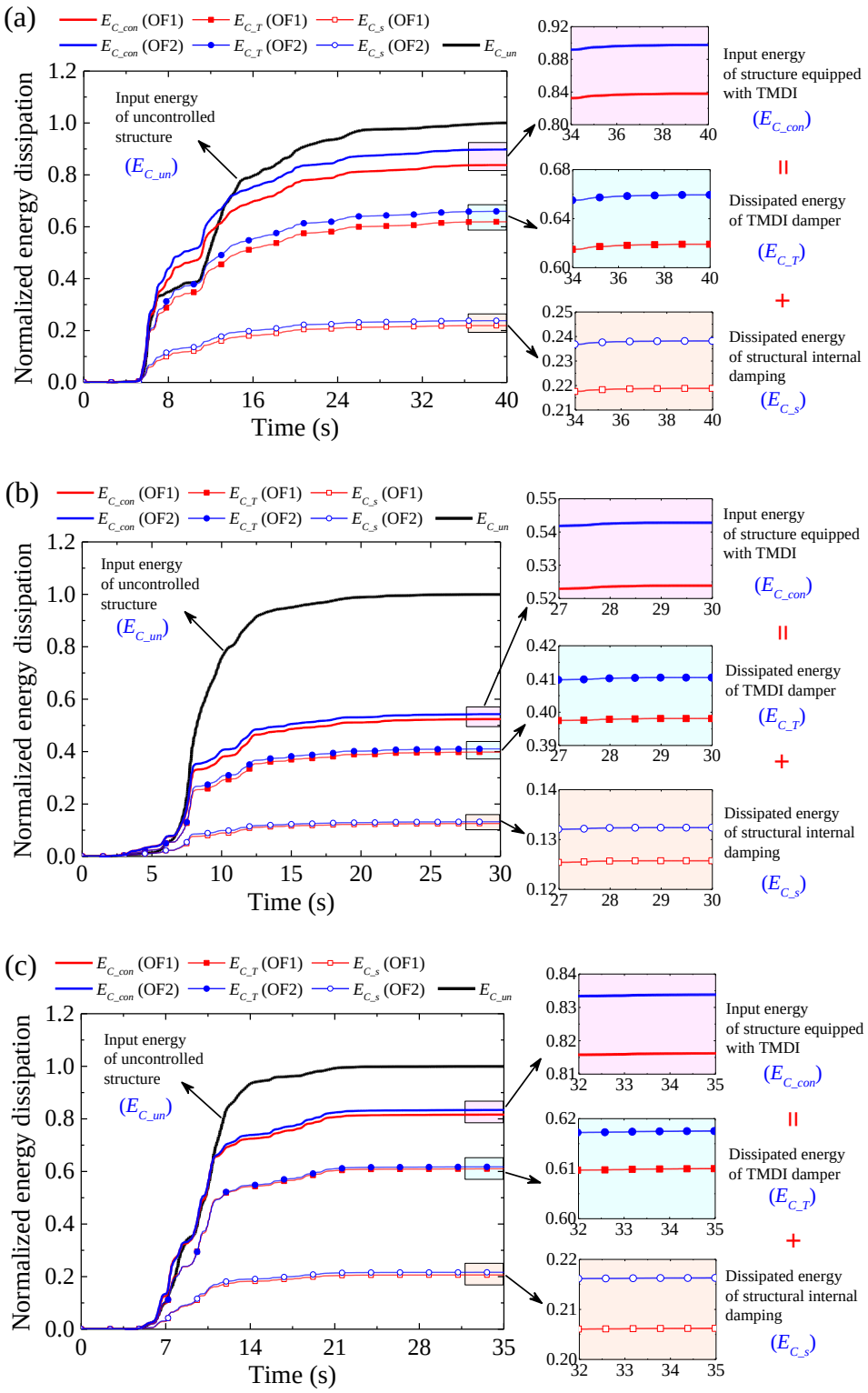

Fig. 16 Normalized accumulated energy dissipated through the TMDI, tuned using the analytical expressions for OF_1 and OF_2. (a) NPNF record #165 (Imperial Valley-06, PGA=0.28*g*); (b) PNF record #1165 (Kocaeli, Turkey, PGA=0.22*g*); (c) FF record #1111 (Kobe, Japan, scaled PGA=0.3*g*).

Overall, numerical data confirm that the use of the analytical optimal tuning expressions in Table 1 render the TMDI a bona fide passive vibration absorber for transient earthquake-induced base

excitations.

7. Concluding remarks

Novel analytically derived closed-form expressions for H_∞-optimal tuning of the TMDI have been presented based on fixed-point theory for arbitrary inerter connectivity in base-excited cantilevered structures modelled by a single (dominant) vibration mode. The derived optimal TMDI stiffness and damping properties minimize the free-end primary structure displacement for harmonic base excitations, assuming no inherent structural damping. The generality and enhanced control performance achieved by the proposed TMDI tuning expressions over previous tuning formulae reported in the literature has been numerically established and discussed for different TMDI configurations including for grounded and non-grounded TMDI configurations. Further, the influence of the assumed dominant vibration mode of the primary structure to the optimal TMDI tuning properties and to the achieved vibration suppression performance has been parametrically quantified for a wide range of TMDI inertial properties. Lastly, the robustness and applicability of the herein derived TMDI tuning expressions for response mitigation of lightly damped primary structures under stationary broadband support excitation as well as under transient earthquake-induced GMs have been demonstrated. The latter involved the numerical assessment of the structural displacement, acceleration, and energy dissipation performance of H_∞-optimal TMDI-equipped lab specimen of a reinforced concrete bridge pier subjected to a suite of 100 recorded earthquake GM records grouped into far-field, near-fault non-pulse, and near-fault pulse-like categories.

Overall, the reported numerical results suggest that the herein derived TMDI tuning formulae endow efficient vibration suppression capability for a much wider range of TMDI configurations and modal primary structure properties than the currently available analytical tuning expressions in the

literature. Still, it is recognized that the assessment of the effectiveness of the proposed TMDI tuning formulae for multi-modal vibration suppression has not been pursued in this study as it is highly structure-and-excitation-dependent. However, it is anticipated that the proposed formulae shall significantly extend the application of TMDI as a bona fide dynamic vibration absorber for base-excited structures by supporting an effective tuning without the need for computationally demanding multi-modal numerical TMDI property optimization under application-specific excitations. This expectation is reinforced by the well-established broadband damping effect of the TMDI [53] whereby higher vibration modes from the targeted one by TMDI tuning are intrinsically suppressed in multi-mode structures.

CRediT authorship contribution statement

Zhenchuan Li: Conceptualization, Software, Methodology, Investigation, Writing – original draft; **Kun Xu:** Conceptualization, Methodology, Investigation, Writing – original draft; **Zixiao Wang:** Investigation, Validation, Writing – review & editing; **Kaiming Bi:** Investigation, Supervision, Writing – review & editing; **Huailei Qin:** Investigation, Validation, Writing – review & editing. **Agathoklis Giaralis:** Investigation, Supervision, Writing – review & editing.

Declaration of Competing Interest

The authors declare that they have no known competing financial interests or personal relationships that could have appeared to influence the work reported in this paper.

Acknowledgements

The authors gratefully acknowledge the support of National Key R&D Program of China (Grant No. 2022YFB2602500) and National Natural Science Foundation of China (52178447). The authors would also like to thank the financial support from the China Scholarship Council (CSC) for

Zhenchuan Li to visit City, University of London, UK (Grant No. 202206540040).

Data availability

Data will be made available on request.

Appendix A. Analytical expressions of objective functions OF1 and OF2

Using Eq. (8), the structural displacement response amplitude over ground displacement excitation amplitude ratio involved in the definition of OF_1 in Eqs. (9) and Eq. (11) can be expressed as

$$\frac{y_{s,0}}{y_{g,0}} = \frac{A + 2i\xi_t B}{C + 2i\xi_t D}, \tag{A.1}$$

with coefficients

$$\begin{aligned} &A = \mu a_1 \Omega^4 + a_4(a_3 v_t^2 - a_3 \Omega^2)\Omega^2,\ B = a_4 a_3 \Omega^3 v_t\ , \\ &C = -a_1^2 \Omega^4 + (1 - a_2\Omega^2 + 2i\Omega\xi_s)(a_3 v_t^2 - a_3 \Omega^2),\ \text{and}\ D = a_3 v_t \Omega(1 - a_2\Omega^2 + 2i\Omega\xi_s), \end{aligned} \tag{A.2}$$

where

$$a_1 = \mu + \beta(1 - \phi(h)),\ a_2 = 1 + \mu + \beta(1 - \phi(h))^2,\ a_3 = \mu + \beta, \text{and}\ a_4 = \gamma + \mu. \tag{A.3}$$

Eqs.(A.1) to (A.3) are used to solve analytically the minimization problem in Eq.(9) by setting ξ_s=0 (undamped primary structure) as detailed in Appendix B, as well as to solve numerically the optimization problem in Eq. (11) for damped primary structures ($\xi_s \neq 0$).

Further, the structural acceleration response amplitude over ground acceleration excitation amplitude ratio involved in the definition of the objective function OF_2 in Eq. (10) and Eq.(12) can be expressed as

$$\frac{\omega_s^2 y_{s,0}}{\ddot{y}_{g,0}} = -\frac{1}{\Omega^2}\frac{A + 2i\xi_t B}{C + 2i\xi_t D} \tag{A.4}$$

with same coefficients given in Eqs.(A.2) and (A.3). Equations (A.2) to (A.4) are used to solve analytically the minimization problem in Eq.(10) by setting ξ_s=0 (undamped primary structure) as discussed in Appendix B, as well as to solve numerically the optimization problem in Eq. (12).

Appendix B. Derivation of optimal TMDI parameters

B.1 Derivation of optimal TMDI frequency ratio

The standard fixed-point theory [65] for treating minimization problems like those in Eqs.(9) and (10) requires that the OF attains the same height at the two fixed frequency ratios Ω_P and Ω_Q, which are TMDI damping independent (see Fig.2). This requirement suffices to determine the optimal TMDI frequency ratio. To this aim, the location of the two specific frequencies is first found by enforcing the condition that the OF value is the same for $\xi_t \to \infty$ and for $\xi_t \to 0$. Focusing on OF_1 and using Eq. (A.1), this condition yields

$$\frac{A^2}{C^2} = \frac{B^2}{D^2} \quad \text{or} \quad AD = \pm BC. \tag{B.1}$$

By using Eqs. (A.2) and (A.3) with Eq. (B.1), one obtains

$$(2a_2a_3a_4 - \mu a_1a_2 - a_1^2a_4) \cdot \Omega^4 - (2a_2a_3a_4v_t^2 + 2a_3a_4 - \mu a_1) \cdot \Omega^2 + 2a_3a_4v_t^2 = 0, \tag{B.2}$$

for the case of $AD = -BC$, and

$$v_t \Omega^5 a_1a_3(\mu - \mu a_2\Omega^2 + a_1a_4\Omega^2) = 0, \tag{B.3}$$

for the case of $AD = +BC$. In the latter case, Eq.(B.3) yields a zero and negative solutions for Ω^2 with no physical meaning for the problem at hand. In this regard, only Eq. (B.2) is used to solve for the two fixed points in the FRF curve.

For this purpose, an expression for the sum of Ω_P^2 and Ω_Q^2 is first found as

$$\Omega_P^2 + \Omega_Q^2 = \frac{2a_2a_3a_4v_t^2 + 2a_3a_4 - \mu a_1}{2a_2a_3a_4 - \mu a_1a_2 - a_1^2a_4}. \tag{B.4}$$

Further, by setting $\xi_t \to \infty$, the FRF values of OF_1 at Ω_P^2 and Ω_Q^2 are determined as

$$\left|\frac{y_{s,0}}{y_{g,0}}\right|_P = \left|\frac{B}{D}\right| = \frac{a_4\Omega_P^2}{1 - a_2\Omega_P^2}, \tag{B.5}$$

and

$$\left|\frac{y_{s,0}}{y_{g,0}}\right|_Q = \left|\frac{B}{D}\right| = \frac{-a_4\Omega_Q^2}{1-a_2\Omega_Q^2}, \tag{B.6}$$

respectively. By setting Eqs. (B.5) and (B.6) to be equal (i.e. enforcing that the FRF curve attains the same height at Ω_P and Ω_Q), one obtains

$$\frac{a_4\Omega_P^2}{1-a_2\Omega_P^2} = \frac{-a_4\Omega_Q^2}{1-a_2\Omega_Q^2}. \tag{B.7}$$

The last equation can be rearranged as

$$\Omega_P^2 + \Omega_Q^2 = 2a_2\Omega_P^2 \cdot \Omega_Q^2. \tag{B.8}$$

Using Eq.(B.2), the product $\Omega_P^2 \cdot \Omega_Q^2$ in the rhs of Eq.(B.8) can be written as

$$\Omega_P^2 \cdot \Omega_Q^2 = \frac{2a_3a_4v_t^2}{2a_2a_3a_4 - \mu a_1a_2 - a_1^2a_4}. \tag{B.9}$$

Next, by substituting Eq. (B.9) into Eq. (B.8), the sum $\Omega_P^2 + \Omega_Q^2$ is expressed by

$$\Omega_P^2 + \Omega_Q^2 = \frac{4a_2a_3a_4v_t^2}{2a_2a_3a_4 - \mu a_1a_2 - a_1^2a_4} \tag{B.10}$$

As a final step, Eqs. (B.4) and (B.10) are combined to yield an analytic formula for the optimal TMDI frequency ratio, $v_{t,opt}$, for OF_1 as

$$v_{t,opt} = \sqrt{\frac{2a_3a_4 - \mu a_1}{2a_2a_3a_4}} \quad (for\ \mathrm{OF}_1) \tag{B.11}$$

By application of the same steps as above, the optimal frequency ratio for OF_2 is found as

$$v_{t,opt} = \sqrt{\frac{2a_2a_3a_4 - \mu a_1a_2 - 2a_1^2a_4}{2a_2^2a_3a_4}} \quad (for\ \mathrm{OF}_2) \tag{B.12}$$

B.2 Derivation of optimal TMDI damping ratio

With the optimal frequency ratio known, the classical fixed-point theory [65] proceeds by requiring that the OF attains local maximum values at the two fixed frequency ratios Ω_P and Ω_Q. This condition allows for determining the optimal damping ratio. For this purpose, knowledge of the FRF values at frequencies Ω_P and Ω_Q is required. For OF_1, this value is determined by first substituting

the optimal frequency ratio of Eq. (B.11) into Eq. (B.2), to reach the quadratic equation

$$(2a_2a_3a_4 - \mu a_1a_2 - a_1^2a_4)\cdot\Omega^4 - (4a_3a_4 - 2\mu a_1)\cdot\Omega^2 + \frac{2a_3a_4 - \mu a_1}{a_2} = 0 \tag{B.13}$$

with roots Ω_P^2 and Ω_Q^2. Then, the roots Ω_P^2 and Ω_Q^2 are determined by solving analytically Eq. (B.13) and the OF_1 value at frequencies Ω_P and Ω_Q is found by substituting Ω_P and Ω_Q into Eq. (B.5) as

$$\left|\frac{y_{s,0}}{y_{g,0}}\right|_{P,Q} = \frac{a_4\left(\sqrt{a_2}(2a_3a_4 - \mu a_1) - a_1\sqrt{a_4(2a_3a_4 - \mu a_1)}\right)}{\sqrt{a_2}\left(a_1\sqrt{a_2a_4(2a_3a_4 - \mu a_1)} - a_1^2a_4\right)} \tag{B.14}$$

Following the same steps as above, the OF_2 value at frequencies Ω_P and Ω_Q is found as

$$\left|\frac{\omega_s^2 y_{s,0}}{\ddot{y}_{g,0}}\right|_{P,Q} = \frac{1}{a_1}\sqrt{a_4(2a_2a_3a_4 - \mu a_1a_2 - a_1^2a_4)} \tag{B.15}$$

With the value of the OF at frequencies Ω_P and Ω_Q known, the optimal damping ratio can be determined by setting the first derivative of the OF squared with respect to Ω^2 equal to zero [68]. For OF_1, the latter operation yields

$$\frac{\partial\left|y_{s,0}/y_{g,0}\right|_{P,Q}^2}{\partial(\Omega^2)} = 0 \Rightarrow \frac{\partial p}{\partial\Omega^2} = \left|\frac{y_{s,0}}{y_{g,0}}\right|_{P,Q}^2 \cdot \frac{\partial q}{\partial\Omega^2}, \tag{B.16}$$

where

$$p = A^2 + (2\xi_t)^2B^2 \; and \; q = C^2 + (2\xi_t)^2D^2. \tag{B.17}$$

Substituting Eq. (B.14) into Eq. (B.16), functional expressions of the square critical TMDI damping ratios at frequencies Ω_P and Ω_Q are obtained which are concisely written as

$$(\xi_t^2)_{P,Q} = f(\mu, \beta, \phi(h), \upsilon_{t,opt}, \Omega_{P,Q}^2) \tag{B.18}$$

since the functional f is too elaborate to report. Finally, the optimal damping ratio $\xi_{t,opt}$ for OF_1 is analytically found as

$$\xi_{t,opt} = a_1\sqrt{\frac{\mu^2a_2 + a_4(5\mu a_1 - 6a_3a_4)}{8a_3a_4[\mu a_1a_2 + a_4(a_1^2 - 2a_2a_3)]}} \quad (for \; OF_1) \tag{B.19}$$

by taking the mean value of ξ_t^2 at the two fixed frequency points P and Q. Following the same steps as above for OF_2, the optimal damping ratio $\xi_{t,opt}$ is analytically found as

$$\xi_{t,opt} = a_1\sqrt{\frac{a_2 a_4(6a_3a_4+\mu a_1)-(\mu a_2)^2-6(a_1a_4)^2}{8a_2a_3a_4(2a_2a_3a_4-\mu a_1a_2-2a_1^2a_4)}} \quad (for\ \mathrm{OF}_2) \tag{B.20}$$

References

[1] R. Ma, K. Bi, H. Hao, Inerter-based structural vibration control: A state-of-the-art review, Eng. Struct., 243 (2021) 112655.

[2] M.Z. Chen, Y. Hu, Inerter and its application in vibration control systems, Springer, 2019.

[3] S. Chowdhury, A. Banerjee, S. Adhikari, A critical review on inertially-amplified passive vibration control devices, Arch. Comput. Methods Eng., (2024) 1-37.

[4] M.C. Smith, Synthesis of mechanical networks: the inerter, IEEE Trans. Automat. Control, 47 (2002) 1648-1662.

[5] L. Marian, A. Giaralis, Optimal design of a novel tuned mass-damper-inerter (TMDI) passive vibration control configuration for stochastically support-excited structural systems, Prob. Eng. Mech., 38 (2014) 156-164.

[6] K. Ikago, K. Saito, N. Inoue, Seismic control of single-degree-of-freedom structure using tuned viscous mass damper, Earthq. Eng. Struct. Dyn., 41 (2012) 453-474.

[7] C. Papageorgiou, N.E. Houghton, M.C. Smith, Experimental testing and analysis of inerter devices, J. Dyn. Syst. Meas. Contr., 131 (2009).

[8] P. Brzeski, M. Lazarek, P. Perlikowski, Experimental study of the novel tuned mass damper with inerter which enables changes of inertance, J. Sound Vib., 404 (2017) 47-57.

[9] D. Pietrosanti, M. De Angelis, A. Giaralis, Experimental study and numerical modeling of nonlinear dynamic response of SDOF system equipped with tuned mass damper inerter (TMDI) tested on shaking table under harmonic excitation, Int. J. Mech. Sci., 184 (2020) 105762.

[10] Z. Li, K. Xu, K. Bi, Q. Han, X. Du, Inerter nonlinearity and its influence on control efficiency of TMDI for suppressing vortex-induced vibration of bridges, J. Bridge Eng., 27 (2022) 04022101.

[11] E.D. John, D.J. Wagg, Design and testing of a frictionless mechanical inerter device using living-

hinges, J. Franklin Inst., 356 (2019) 7650-7668.

[12] A. Gonzalez-Buelga, L. Clare, S. Neild, J. Jiang, D. Inman, An electromagnetic inerter-based vibration suppression device, Smart Mater. Struct., 24 (2015) 055015.

[13] F.C. Wang, M.F. Hong, T.C. Lin, Designing and testing a hydraulic inerter, J. Mech. Eng. Sci., 225 (2010) 66-72.

[14] Y. Shen, Y. Liu, L. Chen, X. Yang, Optimal design and experimental research of vehicle suspension based on a hydraulic electric inerter, Mechatronics, 61 (2019) 12-19.

[15] S. Swift, M.C. Smith, A. Glover, C. Papageorgiou, B. Gartner, N.E. Houghton, Design and modelling of a fluid inerter, Int. J. Control., 86 (2013) 2035-2051.

[16] X. Liu, J.Z. Jiang, B. Titurus, A. Harrison, Model identification methodology for fluid-based inerters, Mech. Syst. Signal Process., 106 (2018) 479-494.

[17] D. De Domenico, P. Deastra, G. Ricciardi, N.D. Sims, D.J. Wagg, Novel fluid inerter based tuned mass dampers for optimised structural control of base-isolated buildings, J. Franklin Inst., 356 (2019) 7626-7649.

[18] M.C. Smith, The inerter: a retrospective, Annu. Rev. Control Robot. Auton. Syst., 3 (2020) 361-391.

[19] H. Garrido, O. Curadelli, D. Ambrosini, Improvement of tuned mass damper by using rotational inertia through tuned viscous mass damper, Eng. Struct., 56 (2013) 2149-2153.

[20] I. Lazar, S. Neild, D. Wagg, Using an inerter-based device for structural vibration suppression, Earthq. Eng. Struct. Dyn., 43 (2014) 1129-1147.

[21] Q. Wang, N.D. Tiwari, H. Qiao, Q. Wang, Inerter-based tuned liquid column damper for seismic vibration control of a single-degree-of-freedom structure, Int. J. Mech. Sci., 184 (2020) 105840.

[22] L. Cao, C. Li, Tuned tandem mass dampers-inerters with broadband high effectiveness for structures under white noise base excitations, Struct. Contr. Health Monit., 26 (2019) e2319.

[23] N. Su, J. Bian, Z. Chen, Y. Xia, A novel lever-type inerter-based vibration absorber, Int. J. Mech. Sci., 254 (2023) 108440.

[24] Z. Li, K. Xu, R. Ma, K. Bi, Q. Han, A novel lever-arm tuned mass damper inerter (LTMDI) for vibration control of long-span bridges, Eng. Struct., 293 (2023) 116662.

[25] Z. Li, R. Ma, K. Xu, Q. Han, Closed-form solutions for the optimal design of lever-arm tuned

mass damper inerter (LTMDI), Mech. Syst. Signal Process., 206 (2024) 110889.

[26] E. Barredo, Z. Zhao, C. Mazón-Valadez, J.M. Larios, I. Maldonado, A grounded inerter-based oscillating TMD for suppressing harmonic and random vibrations, Int. J. Mech. Sci., 254 (2023) 108438.

[27] Z. Jiang, J. Tang, K. Dai, C. Fang, Y. Luo, A tuned cable-inerter system for wind turbine blades vibration suppression, Int. J. Mech. Sci., 269 (2024) 109030.

[28] H. Sun, H. He, Y. Cheng, X. Gao, Theoretical and experimental study on vibration control of a tuned liquid inerter damper with additional damping net and sloped-bottom, Mech. Syst. Signal Process., 213 (2024) 111356.

[29] Z. Zhao, R. Zhang, Y. Jiang, C. Pan, A tuned liquid inerter system for vibration control, Int. J. Mech. Sci., 164 (2019) 105171.

[30] F. Petrini, A. Giaralis, Z. Wang, Optimal tuned mass-damper-inerter (TMDI) design in wind-excited tall buildings for occupants' comfort serviceability performance and energy harvesting, Eng. Struct., 204 (2020) 109904.

[31] J. Dai, Z.-D. Xu, P.-P. Gai, Tuned mass-damper-inerter control of wind-induced vibration of flexible structures based on inerter location, Eng. Struct., 199 (2019) 109585.

[32] Z. Zhu, W. Lei, Q. Wang, N. Tiwari, B. Hazra, Study on wind-induced vibration control of linked high-rise buildings by using TMDI, J. Wind Eng. Ind. Aerodyn., 205 (2020) 104306.

[33] Z. Wang, A. Giaralis, Top-story softening for enhanced mitigation of vortex shedding-induced vibrations in wind-excited tuned mass damper inerter-equipped tall buildings, J. Struct. Eng., 147 (2021) 04020283.

[34] K. Xu, Q. Dai, K. Bi, G. Fang, Y. Ge, Closed-form design formulas of TMDI for suppressing vortex-induced vibration of bridge structures, Struct. Contr. Health Monit., 29 (2022) e3016.

[35] K. Xu, K. Bi, Q. Han, X. Li, X. Du, Using tuned mass damper inerter to mitigate vortex-induced vibration of long-span bridges: Analytical study, Eng. Struct., 182 (2019) 101-111.

[36] Z. Li, K. Xu, K. Bi, L. Xu, Q. Han, Suppressing wind-induced bending and torsional vibrations of long-span bridges by series-type tuned mass damper inerters (STMDIs), Struct, 48 (2023) 918-933.

[37] K. Xu, Q. Dai, K. Bi, G. Fang, L. Zhao, Multi-mode vortex-induced vibration control of long-span bridges by using distributed tuned mass damper inerters (DTMDIs), J. Wind Eng. Ind.

Aerodyn., 224 (2022) 104970.

[38] Z. Zhang, B. Fitzgerald, Tuned mass-damper-inerter (TMDI) for suppressing edgewise vibrations of wind turbine blades, Eng. Struct., 221 (2020) 110928.

[39] S. Sarkar, B. Fitzgerald, Vibration control of spar-type floating offshore wind turbine towers using a tuned mass-damper-inerter, Struct. Contr. Health Monit., 27 (2020) e2471.

[40] R. Ruiz, A. Taflanidis, A. Giaralis, D. Lopez-Garcia, Risk-informed optimization of the tuned mass-damper-inerter (TMDI) for the seismic protection of multi-storey building structures, Eng. Struct., 177 (2018) 836-850.

[41] A. Kaveh, M.F. Farzam, H.H. Jalali, Statistical seismic performance assessment of tuned mass damper inerter, Struct. Contr. Health Monit., 27 (2020) e2602.

[42] D. Patsialis, A. Taflanidis, A. Giaralis, Tuned-mass-damper-inerter optimal design and performance assessment for multi-storey hysteretic buildings under seismic excitation, Bull. Earthquake Eng., (2021) 1-36.

[43] K. Rajana, Z. Wang, A. Giaralis, Optimal design and assessment of tuned mass damper inerter with nonlinear viscous damper in seismically excited multi-storey buildings, Bull. Earthquake Eng., (2023) 1-31.

[44] G. Alotta, C. Biondo, A. Giaralis, G. Failla, Seismic protection of land-based wind turbine towers using the tuned inerter damper, Structures, 51 (2023) 640-656.

[45] D. De Domenico, G. Ricciardi, An enhanced base isolation system equipped with optimal tuned mass damper inerter (TMDI), Earthq. Eng. Struct. Dyn., 47 (2018) 1169-1192.

[46] M. De Angelis, A. Giaralis, F. Petrini, D. Pietrosanti, Optimal tuning and assessment of inertial dampers with grounded inerter for vibration control of seismically excited base-isolated systems, Eng. Struct., 196 (2019) 109250.

[47] D. Pietrosanti, M. De Angelis, A. Giaralis, Experimental seismic performance assessment and numerical modelling of nonlinear inerter vibration absorber (IVA)-equipped base isolated structures tested on shaking table, Earthq. Eng. Struct. Dyn., 50 (2021) 2732-2753.

[48] L. Zhang, R. Zhang, L. Xie, S. Xue, Dynamics and isolation performance of a vibration isolator with a yoke-type nonlinear inerter, Int. J. Mech. Sci., 254 (2023) 108447.

[49] X. Jin, M.Z. Chen, Z. Huang, Minimization of the beam response using inerter-based passive

vibration control configurations, Int. J. Mech. Sci., 119 (2016) 80-87.

[50] Y. Hu, M.Z. Chen, Performance evaluation for inerter-based dynamic vibration absorbers, Int. J. Mech. Sci., 99 (2015) 297-307.

[51] D. Pietrosanti, M. De Angelis, M. Basili, A generalized 2-DOF model for optimal design of MDOF structures controlled by Tuned Mass Damper Inerter (TMDI), Int. J. Mech. Sci., 185 (2020) 105849.

[52] G.B. Warburton, Optimum absorber parameters for various combinations of response and excitation parameters, Earthq. Eng. Struct. Dyn., 10 (1982) 381-401.

[53] A. Giaralis, A. Taflanidis, Optimal tuned mass-damper-inerter (TMDI) design for seismically excited MDOF structures with model uncertainties based on reliability criteria, Struct. Contr. Health Monit., 25 (2018) e2082.

[54] A.A. Taflanidis, A. Giaralis, D. Patsialis, Multi-objective optimal design of inerter-based vibration absorbers for earthquake protection of multi-storey building structures, J. Franklin Inst., 356 (2019) 7754-7784.

[55] D. Pietrosanti, M. De Angelis, M. Basili, Optimal design and performance evaluation of systems with Tuned Mass Damper Inerter (TMDI), Earthq. Eng. Struct. Dyn., 46 (2017) 1367-1388.

[56] D. De Domenico, G. Ricciardi, Optimal design and seismic performance of tuned mass damper inerter (TMDI) for structures with nonlinear base isolation systems, Earthq. Eng. Struct. Dyn., 47 (2018) 2539-2560.

[57] Z. Wang, A. Giaralis, Enhanced motion control performance of the tuned mass damper inerter through primary structure shaping, Struct. Contr. Health Monit., 28 (2021) e2756.

[58] N. Su, J. Bian, S. Peng, Y. Xia, Generic optimal design approach for inerter-based tuned mass systems, Int. J. Mech. Sci., 233 (2022) 107654.

[59] Z. Zhang, B. Chen, X. Hua, Closed-form optimization of tuned mass-damper-inerter (TMDI) in flexible structures, J. Build. Eng., 72 (2023) 106554.

[60] B. Chen, Z. Zhang, X. Hua, Equal modal damping-based optimal design of a grounded tuned mass-damper-inerter for flexible structures, Struct. Contr. Health Monit., 29 (2022) e3106.

[61] L. Marian, A. Giaralis, The tuned mass-damper-inerter for harmonic vibrations suppression, attached mass reduction, and energy harvesting, Smart Struct. Syst., 19 (2017) 665-678.

[62] A. Di Matteo, C. Masnata, A. Pirrotta, Simplified analytical solution for the optimal design of tuned mass damper inerter for base isolated structures, Mech. Syst. Signal Process., 134 (2019) 106337.

[63] C. Masnata, A. Di Matteo, C. Adam, A. Pirrotta, Smart structures through nontraditional design of Tuned Mass Damper Inerter for higher control of base isolated systems, Mech. Res. Commun., 105 (2020) 103513.

[64] D.K. Pandey, S.K. Mishra, Inerter assisted robustness of compliant liquid column damper, Struct. Contr. Health Monit., 28 (2021) e2763.

[65] J.P. Den Hartog, Mechanical vibrations, 4th edition, McGraw-Hall Book Company, New York, 1956.

[66] A.T. Council, Quantification of building seismic performance factors, US Department of Homeland Security, FEMA, 2009.

[67] H.C. Tsai, G.C. Lin, Optimum tuned-mass dampers for minimizing steady-state response of support-excited and damped systems, Earthq. Eng. Struct. Dyn., 22 (1993) 957-973.

[68] W.O. Wong, Y. Cheung, Optimal design of a damped dynamic vibration absorber for vibration control of structure excited by ground motion, Eng. Struct., 30 (2008) 282-286.

[69] L. Marian, The tuned mass damper inerter for passive vibration control and energy harvesting in dynamically excited structural systems, in, City University London, 2015.

[70] A. Ghosh, B. Basu, A closed-form optimal tuning criterion for TMD in damped structures, Struct. Contr. Health Monit., 14 (2007) 681-692.

[71] N. Su, Y. Xia, S. Peng, Filter-based inerter location dependence analysis approach of Tuned mass damper inerter (TMDI) and optimal design, Eng. Struct., 250 (2022) 113459.

[72] H. Qin, K. Bi, H. Dong, Q. Han, X. Du, Shake table tests on RC double-column bridge piers with self-centering energy dissipation braces, J. Bridge Eng., 28 (2023) 04023049.

[73] M. De Angelis, F. Petrini, D. Pietrosanti, Optimal design of the ideal grounded tuned mass damper inerter for comfort performances improvement in footbridges with practical implementation considerations, Struct. Contr. Health Monit., 28 (2021) e2800.

[74] D. Patsialis, A. Taflanidis, A. Giaralis, Exploring the impact of excitation and structural response/performance modeling fidelity in the design of seismic protective devices, Eng. Struct., 291

(2023) 115811.

[75] C.-M. Uang, V.V. Bertero, Use of energy as a design criterion in earthquake-resistant design, Earthquake Engineering Research Center, University of California Berkeley, 1988.

[76] Z. Zhao, R. Zhang, C. Pan, Q. Chen, Y. Jiang, Input energy reduction principle of structures with generic tuned mass damper inerter, Struct. Contr. Health Monit., 28 (2021) e2644.